DMD Fast Forward. Published on September 14, 2017 as DOI: 10.1124/dmd.117.076851
This article has not been copyedited and formatted. The final version may differ from this version.

DMD # 76851

Physiologically-based pharmacokinetic model predictions of panobinostat (LBH589) as a victim and perpetrator of drug-drug interactions

Heidi J. Einolf, Wen Lin, Christina S. Won, Lai Wang, Helen Gu, Dung Y. Chun, Handan He, James B. Mangold

Pharmacokinetic Sciences, Novartis Institutes for Biomedical Research, East Hanover, New Jersey, USA

DMD # 76851

Running Title:

PBPK Prediction of Panobinostat Drug-Drug Interactions

Corresponding Author:

Corresponding Author:

Heidi J. Einolf, Ph.D.

Novartis, One Health Plaza, East Hanover, NJ 07936; Phone: +1-862-778-3119, Fax: +1-973-781-5023. Email: heidi.einolf@novartis.com

Number of text pages: 33

Number of tables: 10

Number of figures: 9

Number of references: 38

Number of words in Abstract: 249

Number of words in Introduction: 748

Number of words in Discussion: 1500

Abbreviations:

ADME, absorption, distribution, metabolism, and excretion

ACAT, advanced compartmental absorption and transit

AUC, area under the concentration-time curve

B/P, blood to plasma ratio

CI, confidence interval

CL, clearance

CL_{int}, intrinsic clearance

$CL_{int,u}$, unbound intrinsic clearance

C_{max}, maximal concentration

CL_R, renal clearance

CYP, cytochrome P450

DEX, dexamethasone

DDI, drug-drug interactions

EMA, European Medicines Agency

FDA, Food and Drug Administration

f_a, fraction of dose absorbed

fu_{gut}, unbound fraction in the gut

fu_{mic}, unbound fraction in microsomes

fu_{plasma}, unbound fraction in plasma

GI, gastrointestinal

HLM, human liver microsomes

HPLC, high-performance liquid chromatography

k_a, absorption rate constant

K_i, inhibition constant

K_m, Michaelis-Menten constant

$K_{m,u}$ unbound Michaelis-Menten constant (corrected by fu_{mic})

KTZ, ketoconazole

PBPK, physiologically-based pharmacokinetics

$P_{eff,man}$, effective permeability in man

PK, pharmacokinetics

q.d., once a day dosing

Q_{gut}, nominal flow through the gut

RAF, relative activity factor

RIF, rifampin

SD, standard deviation

T_{max}, time to reach maximum concentration

V_{max}, maximum velocity

V_{ss}, volume of distribution at steady-state

Abstract

Panobinostat (Farydak®) is an orally active hydroxamic acid derived histone deacetylase inhibitor for the treatment of relapsed/refractory multiple myeloma. Based upon recombinant cytochrome P450 (CYP) kinetic analyses *in vitro*, panobinostat oxidative metabolism in human liver microsomes was found to be primarily mediated by CYP3A4 with lower contributions by CYP2D6 and CYP2C19. Panobinostat was also shown to be an *in vitro* reversible and time-dependent inhibitor of CYP3A4/5, and a reversible inhibitor of CYP2D6 and CYP2C19. Based upon a previous clinical drug-drug interaction study with ketoconazole (KTZ), the contribution of CYP3A4 *in vivo* was estimated to be ~40%. Using clinical pharmacokinetic (PK) data from several trials including the KTZ DDI study, a physiologically-based pharmacokinetic (PBPK) model was built to predict panobinostat PK after single and multiple doses (within 2-fold of observed values for most trials) and the clinical DDI with KTZ (predicted and observed AUC ratios of 1.8). The model was then applied to predict the drug interaction with the strong CYP3A4 inducer, rifampin (RIF) and sensitive CYP3A4 substrate, midazolam (MDZ) *in lieu* of clinical trials. Panobinostat exposure was predicted to decrease in the presence of RIF (65%) and inconsequentially increase MDZ exposure (4%). Additionally, PBPK modeling was used to examine the effects of stomach pH on the absorption of panobinostat in humans. The absorption of panobinostat is not expected to be affected by increases in stomach pH. The results from these studies were incorporated into the FDA-approved product label, providing guidance for Farydak® dosing recommendations when combined with other drugs.

DMD Fast Forward. Published on September 14, 2017 as DOI: 10.1124/dmd.117.076851
This article has not been copyedited and formatted. The final version may differ from this version.

Introduction

Panobinostat (Farydak®, formerly LBH589) is an orally active hydroxamic acid derived histone deacetylase (HDAC) inhibitor for the treatment of relapsed and refractory multiple myeloma (MM). Panobinostat was approved recently by the US Food and Drug Administration (FDA) and European Medicines Agency (EMA) as a combination therapy with bortezomib and dexamethasone (DEX) in patients with relapsed/refractory MM who have received at least two prior therapies containing an immunomodulatory agent and bortezomib. HDAC enzymes catalyze the deacetylation of lysine residues on histones and prevent transcription of genes encoding proteins involved in cell cycle regulation, differentiation and apoptosis (reviewed in Garnock-Jones 2015). Inhibition of HDAC enzymes by drugs like panobinostat causes an increase in histone acetylation, leading to cellular responses such as cell cycle arrest, apoptosis, and delays in mitosis (reviewed in Cheng et al., 2015). The molecular structure of panobinostat is shown in Fig. 1.

Panobinostat is considered a biopharmaceutics classification system Class I/II -like drug. It is highly permeable and rapidly absorbed after an oral dose in cancer patients with peak levels occurring within 2h (Farydak® prescribing information, 2016 and FDA Clinical Pharmacology Review, 2015). The systemic clearance (CL) was estimated to be 33 L/hr based on population pharmacokinetic (PK) analysis (Savelieva et al., 2015). There is a high first-pass CL with an absolute bioavailability of ~21% (Farydak® prescribing information, 2016). The absorption of panobinostat is altered when the drug is taken with a high-fat meal; 44% reduction in C_{max} and delayed T_{max} of 1-1.5h, but the AUC is minimally impacted (Shapiro et al., 2012). Solubility of panobinostat lactate anhydrous is pH-dependent, with the highest solubility in buffer pH 3.0 and low solubility at pH 7.6 (Farydak® prescribing information, 2016 and FDA Clinical

Pharmacology Review, 2015). Currently, there are no clinical studies examining an increase of pH on the PK of panobinostat. In the radiolabeled human absorption, disposition, metabolism, and excretion (ADME) study, 44-77% of the oral [^{14}C]-panobinostat dose was recovered in the feces and 29-51% was excreted in urine (Clive et al., 2012). The main elimination pathway of panobinostat in humans was determined to be metabolism, as the mean unchanged panobinostat recovered in urine was only 1.9% of the dose and presence of panobinostat in the feces was found in only one patient (~3.3% of the dose). The minimal recovery of parent drug in feces suggested near-complete oral absorption of panobinostat. The metabolism of panobinostat was extensive in humans; at least 77 distinct metabolites were identified with ~40 observed circulating in plasma (Clive et al., 2012). The prominent metabolic pathways of panobinostat included reduction and hydrolysis of the hydroxamic acid and one- and two-carbon shortening of this side chain, as well as mono-oxygenation, and glucuronidation. Based upon the identity of the metabolites present in the excreta, cytochrome P450 (CYP)-mediated oxidative CL was estimated to range from a maximum of 30-47% of the dose (Clive et al., 2012). This data was consistent with the resultant effect of the CYP3A4 strong inhibitor, ketoconazole (KTZ) on panobinostat exposure in patients (increase AUC of 1.8-fold and C_{max} of 1.6-fold), suggesting CYP3A4 contribution to total panobinostat CL is ~40% (Hamberg et al., 2011).

The purpose of this manuscript is to present the studies and results identifying the CYP enzyme(s) involved in the oxidative metabolism of panobinostat in human liver and determination of their relative contributions *in vitro* and scaled contributions *in vivo*. In addition, the *in vitro* CYP drug-drug interaction (DDI) properties (inhibition and induction) of panobinostat are presented. Based upon these results, as well as the clinical results of the human radiolabeled ADME study (Clive et al., 2012) and clinical drug interaction with KTZ (Hamberg

et al., 2011), a physiologically-based pharmacokinetic (PBPK) model using the Simcyp® Simulator was constructed using panobinostat physiochemical properties, absorption, distribution, and CL properties optimized from modelling clinical PK data. This PBPK model was then verified to predict the interaction of panobinostat with the weak CYP3A4 inducer, DEX, and then used to predict clinically untested scenarios: the effect of panobinostat with the strong CYP3A4 inducer, rifampin (RIF), as well as the drug interaction with the sensitive CYP3A4 substrate, midazolam (MDZ). In addition, an Advanced Compartmental Absorption and Transit (ACAT™) PBPK model for panobinostat was built using GastroPlus™ to evaluate the effects of changing pH (*e.g.* as with co-administration of acid reducing agents) on the absorption of panobinostat in humans. We describe herein how these *in vitro* DDI studies and PBPK modelling results helped to define the FDA-approved product label language regarding drug interaction and dosing recommendations for Farydak®.

DMD Fast Forward. Published on September 14, 2017 as DOI: 10.1124/dmd.117.076851
This article has not been copyedited and formatted. The final version may differ from this version.

Materials and methods

Materials

[^{14}C]Panobinostat was synthesized in-house (Novartis, East Hanover, NJ). The specific activity was 50-52 mCi/mmol with >95% radiochemical purity. Pooled human liver microsomes (HLM) were purchased from XenoTech, LLC (Kansas City, KS) and Corning Gentest (Tewksbury, MA). Cryopreserved hepatocytes were purchased from BioreclamationIVT (Baltimore, MD) and Corning Gentest. Recombinant human CYP and UDP-glucuronosyltransferase (UGT) enzymes, hydroxybupropion, 6α-hydroxypaclitaxel, 4'-hydroxydiclofenac, 4'-hydroxy-*S*-mephenytoin, *N*-desethylamodiaquine, and *S*-mephenytoin, were also purchased from Corning Gentest. The following chemicals were obtained from Sigma-Aldrich (St. Louis, MO): 6β-hydroxytestosterone, acetaminophen, alamethicin, ammonium acetate, amodiaquine, β-napthoflavone (BNF), bupropion, chlorzoxazone, diclofenac, dimethyl sulfoxide, furafylline, gemfibrozil glucuronide, midazolam, $MgCl_2$, MTT (3-[4,5-dimethylthiazol-2-yl]-2,5-diphenyl tetrazolium bromide), NADPH, paclitaxel, paroxetine, perchloric acid, phenacetin, phenobarbital (PB), potassium phosphate (mono- and di-basic), rifampicin (RIF), testosterone, ticlopidine, troleandomycin, and UDPGA. Bufuralol hydrochloride, 1'-hydroxybufuralol maleate, 6-hydroxychlorzoxazone, *S*-mephenytoin, 4'-hydroxy-*S*-mephenytoin and 1'-hydroxy-midazolam were obtained from Ultrafine Chemicals (Manchester, UK). Tienilic acid was obtained internally at Novartis. Acetonitrile, formic acid, and methanol were purchased from Fisher Scientific Co. (Pittsburgh, PA). IN FLOW 2:1 was purchased from LabLogic Systems, Inc. (Brandon, FL).

In Vitro CYP Inhibition

DMD Fast Forward. Published on September 14, 2017 as DOI: 10.1124/dmd.117.076851
This article has not been copyedited and formatted. The final version may differ from this version.

The potential for reversible and/or time-dependent inhibition of CYP1A2, CYP2B6, CYP2C8, CYP2C9, CYP2C19, CYP2D6, CYP2E1, and CYP3A4/5 by panobinostat was investigated *in vitro* using pooled HLM (mixed gender, n = 50, XenoTech, LLC or n = 150, Corning Gentest). CYP activity was assessed using the probe reactions, phenacetin *O*-deethylation (CYP1A2), bupropion hydroxylation (CYP2B6), paclitaxel 6α-hydroxylation or *N*-deethylamodiaquine (CYP2C8), diclofenac 4'-hydroxylation (CYP2C9), *S*-mephenytoin 4'-hydroxylation (CYP2C19), bufuralol 1'-hydroxylation (CYP2D6), chlorzoxazone 6-hydroxylation (CYP2E1), and midazolam-1′-hydroxylation and testosterone 6β-hydroxylation (CYP3A4/5). For reversible inhibition, incubations (37°C, 10-30 min) were composed of (final concentrations): potassium phosphate buffer (100 mM, pH 7.4), NADPH (1 mM), $MgCl_2$ (5 mM), HLM protein (0.05-0.5 mg protein/ml), probe substrate (5 μM phenacetin, diclofenac, bufuralol, or MDZ, 10 μM paclitaxel or chlorzoxazone, 15 μM *S*-mephenytoin, or 25 μM bupropion or testosterone), varying concentrations of panobinostat (0-100 μM) and organic solvent (<1.5%). The reactions were run in triplicate. After a 3 min thermal equilibration, the reactions were initiated by addition of NADPH and terminated by addition of acetonitrile (2 volumes). Reactions were previously shown to be linear with respect to time and protein concentration (results not shown). Formation of probe substrate metabolites from the above samples: acetaminophen, hydroxybupropion, 6α-hydroxypaclitaxel or *N*-deethylamodiaquine, 4'-hydroxydiclofenac, 4'-hydroxy-*S*-mephenytoin, 1'-hydroxybufuralol, 6-hydroxychlorzoxazone, 1′-hydroxymidazolam, or 6β-hydroxytestosterone was determined by liquid chromatography-tandem mass spectrometry (LC-MS/MS) after concentration and reconstitution of the samples in acetonitrile/water containing an internal standard. IC_{50} values for the inhibition of CYP enzyme were determined by visual inspection of the data (% of control CYP activity vs. panobinostat

DMD Fast Forward. Published on September 14, 2017 as DOI: 10.1124/dmd.117.076851
This article has not been copyedited and formatted. The final version may differ from this version.

concentration). Due to the low IC_{50} value associated with CYP2D6 inhibition, the corresponding apparent K_i value was determined for burfuralol 1'-hydroxylation activity. The incubations were carried out as described above with varying concentrations of bufuralol (0.5-10 µM) and panobinostat (0-0.2 µM). The K_i value was determined by non-linear regression analysis using an equation for competitive inhibition: $v = V_{max}[S]/(K_m\ (1+[I]/K_i)+[S])$, where v is the initial velocity, V_{max} is the maximum velocity, K_m is the Michaelis Menten constant, [S] is the substrate concentration, [I] is the inhibitor concentration, and K_i is the inhibition constant.

For assessments of time-dependent inhibition of CYP1A2, CYP2B6, CYP2C8, CYP2C9, CYP2C19, CYP2D6, or CYP3A4/5 activity, panobinostat (0-50 or 0-100 µM) was pre-incubated (37°C) with HLM (0.5 or 1 mg microsomal protein/ml) in the same buffer components as described above (in duplicates). The pre-incubations were initiated by addition of NADPH. After various pre-incubation times, aliquots were removed and transferred to an enzyme activity assay mixture (20-fold dilution of the pre-incubation reaction) containing the same buffer components as the pre-incubation and CYP probes substrates to determine activity remaining. The concentrations of probe substrates in the enzyme activity assay were 100 µM phenacetin (CYP1A2), 1.5 mM bupropion (CYP2B6), 20 µM amodiaquine (CYP2C8), 50 µM diclofenac (CYP2C9), 300 µM *S*-mephenytoin (CYP2C19), 50 µM bufuralol (CYP2D6), and 20 µM MDZ (CYP3A4/5). The enzyme activity assay reactions were incubated at 37°C for 6-8 min and the reaction terminated as above. Positive control time-dependent inhibitors included furafylline (CYP1A2), ticlopidine (CYP2B6 and CYP2C19), gemfibrozil glucuronide (CYP2C8), tienilic acid (CYP2C9), paroxetine (CYP2D6), and troleandomycin (CYP3A4/5). Preparation of the samples for analysis of the probe substrate metabolite formation by LC-MS/MS was as described above. The inactivation parameters, k_{inact} (maximum inactivation rate) and K_I (concentration at

DMD Fast Forward. Published on September 14, 2017 as DOI: 10.1124/dmd.117.076851
This article has not been copyedited and formatted. The final version may differ from this version.

½ k_{inact}), were determined by plotting the natural log of the percentage of control activity remaining following incubations with increasing inhibitor concentration, plotted against the time of the pre-incubation. The absolute value of the observed rate of inactivation (k_{obs}) was then plotted against the inhibitor concentration and the data analyzed by non-linear regression using the equation: $k_{obs} = k_{inact}[I]/K_I+[I]$.

In Vitro CYP Induction

The potential for induction of CYP1A2, CYP2B6, CYP2C9, and CYP3A4 mRNA and enzyme activities by panobinostat was assessed *in vitro* using cryopreserved hepatocytes from three donors. The cells were treated with panobinostat (0.01, 0.1, or 1 µM), the positive controls, RIF (0.01, 0.1, 1, or 10 µM), PB (1 mM), or BNF (10 µM), and the vehicle control (0.1% dimethyl sulfoxide) for 72 h. The media was changed with fresh addition of the compounds or vehicle control 24 h after the first treatment dose. Induction of mRNA was determined by real-time polymerase chain reaction (PCR) using the Comparative C_T Method, enzyme activity was measured *in situ* using CYP-selective probe substrates, and cell viability was assessed using the MTT (3-[4,5-dimethylthiazol-2-yl]-2,5-diphenyl tetrazolium bromide, Sigma-Aldrich) assay after the treatment period. The method was as essentially described in Flarakos et al., 2016.

In vitro CYP Reaction Phenotyping

In vitro metabolism. The metabolism of [^{14}C]panobinostat was examined in pooled HLM (mixed gender, n = 46, Corning Gentest) in presence of NADPH and/or UDPGA. HLM (1 mg protein/ml) in 100 mM potassium phosphate buffer (pH 7.4) were pre-incubated with alamethicin (60 µg alamethicin·mg protein^{-1}, final concentration) for 15 min on ice. $MgCl_2$ (5 mM, final concentration) and [^{14}C]panobinostat (39 µM, final concentration) were then added and the samples and thermally equilibrated at 37ºC for 3 min. The reactions (in singlet) were

DMD Fast Forward. Published on September 14, 2017 as DOI: 10.1124/dmd.117.076851
This article has not been copyedited and formatted. The final version may differ from this version.

initiated with 4 mM UDPGA and/or 1 mM NADPH (final concentrations) and the samples were incubated for 30 min at 37°C. Control incubations did not contain co-factors. The reactions were terminated by the addition of 1/20 volume of cold 35% perchloric acid to avoid excessive dilution of the sample to improve radiochemical detection sensitivity. The precipitated protein was removed by centrifugation at 39,000 x *g* for 10 min at ~4°C in an Avante 30 high speed microcentrifuge (Beckman Coulter, Fullerton, CA). Aliquots of the supernatants were analyzed by reversed-phase high-performance liquid chromatography (HPLC). The HPLC chromatographic equipment consisted of a Waters 2695 Separations module, equipped with an autosampler and quaternary pump system (Waters, Milford, MA). The chromatographic separation was performed on a Phenomenex Synergy Hydro RP column (150 x 4.6 mm, 4 µm) at a temperature of 30°C (Phenomenex, Torrance, CA). Gradient elution consisted of solvent A (10 mM ammonium acetate, 0.1% formic acid, v/v, pH 3.5) and solvent B (acetonitrile/methanol, 82/18, *v*/*v*) at a flow rate of 1 ml/min. The elution was as follows: 0-10% B (0 to 10 min), 10-18.5% B (10 to 27 min), 18.5-29.5% B (27-45 min), 29.5-100% B (45-52 min). Radioactivity was measured in-line with a β-RAM radioactivity detector (Lablogic Systems Inc., Brandon, FL) with addition of 3 mL liquid scintillant/min (IN FLOW 2:1, Lablogic Systems Inc.) to the HPLC eluate. Chromatograms were evaluated using Winflow HPLC application software (Version 1.4a, Lablogic Systems Inc.).

Enzyme identification. To identify the CYP enzyme(s) involved in the metabolism of panobinostat in humans, [^{14}C]panobinostat (39 µM, final concentration) was incubated with the recombinant human (rh) CYP enzymes: CYP1A1, CYP1A2, CYP1B1, CYP2A6, CYP2B6, CYP2C8, CYP2C9, CYP2C18, CYP2C19, CYP2D6, CYP2E1, CYP2J2, CYP3A4, CYP3A5, CYP4A11 (100 pmol CYP/ml) or control microsomes in 100 mM potassium phosphate buffer

(pH 7.4) containing 5 mM $MgCl_2$, final concentrations. The reactions (in singlet) were thermally equilibrated at 37°C and initiated by the addition of NADPH (1 mM, final concentration). The samples were incubated for 30 min at 37°C and were quenched, processed, and analyzed by HPLC with in-line radioactivity detection, as described above.

Relative contributions of CYP enzymes. The relative contributions of CYP2C19, CYP2D6 and CYP3A4 enzymes to the *in vitro* hepatic oxidative CL of panobinostat were determined by rhCYP kinetics and scaling of the enzyme efficiencies to human liver microsomal CL. CYP2C19 (25 pmol CYP/ml, 0.20 mg microsomal protein/ml), CYP2D6 (25 pmol CYP/ml, 0.24 mg microsomal protein/ml), CYP3A4 (50 pmol CYP/ml, 0.26 mg microsomal protein/ml) were pre-incubated with varying concentrations of [^{14}C]panobinostat (in duplicate) in potassium phosphate buffer with $MgCl_2$ for 3 min. The reactions were initiated with NADPH and were incubated at 37°C for 5 min for rhCYP2D6 incubations and up to 10 and 20 min for rhCYP2C19 and rhCYP3A4 incubations, respectively. Control samples at each concentration of [^{14}C]panobinostat were prepared using control microsomes at the same protein concentration. The samples were quenched, processed, and analyzed by HPLC as described above or with off-line low level radioactivity counting. For the low level counting, the HPLC eluate was collected with a fraction collector (FC204 Gilson Inc., Middleton, WI) at 0.25 min per fraction into Deepwell LumaPlate-96 plates (PerkinElmer Life and Analytical Sciences). The fractions were dried with a stream of nitrogen and radioactivity was counted with a TopCount NXT Microplate Scintillation and Luminescence Counter (PerkinElmer Life and Analytical Sciences) with a counting time of 10 min per well. For calculation of metabolism activity in all kinetic studies, the amount of radioactivity present in impurity peaks identified in the control incubations that co-eluted with actual metabolites were subtracted out from the identical peaks in the reaction

DMD Fast Forward. Published on September 14, 2017 as DOI: 10.1124/dmd.117.076851
This article has not been copyedited and formatted. The final version may differ from this version.

incubations. To determine the metabolism activity of [^{14}C]panobinostat, the percent of radioactivity of each peak in the HPLC chromatogram was quantified (totaling 100%). The amount of specific metabolites formed in the reaction was based upon the percentage of radioactivity in the product peak with respect to the total amount of [^{14}C]panobinostat in the starting reaction. The metabolism activity was therefore calculated as the amount of product formed per total amount of CYP enzyme in the reaction per reaction time (*i.e.* nmol metabolite formed/nmol CYP enzyme/h).

[^{14}C]Panobinostat metabolism activity was plotted against substrate concentration and the kinetic parameters, K_m and V_{max} values were determined by non-linear regression analysis using the Michaelis Menten equation: $v = V_{max}[S]/(K_m+[S])$. Total [^{14}C]panobinostat metabolism remained $\sim\leq$ 20% for all reactions. To estimate the relative contribution of CYP2C19, CYP2D6, and CYP3A4 to the metabolism of panobinostat in HLM, a relative activity factor (RAF) was determined. The RAF is the ratio of a specific CYP activity in the recombinant expressed microsomes versus the same specific CYP activity in the pooled HLM under substrate saturating conditions. The relative activity factors for CYP2C19, CYP2D6, and CYP3A4 were determined by comparison of probe substrate metabolism activities (determined by the vendor): *S*-mephenytoin 4'-hydroxylase activities in pooled HLM (56 pmol/mg protein/min) and rhCYP2C19 (22 pmol/pmol CYP/min or 2750 pmol/mg protein/min), bufuralol 1'-hydroxylase activities in HLM (94 pmol/mg protein/min) and rhCYP2D6 (47 pmol/pmol CYP/min or 4841 pmol/mg protein/min), and testosterone 6β-hydroxylase activities (CYP3A4/5) in HLM (4300 pmol/mg protein/min) and rhCYP3A4 (180 pmol/pmol CYP/min or 35,280 pmol/mg protein/min). The relative activity factors were determined to be 49.1 for rhCYP2C19

[as rhCYP2C19 was 49.1-fold more active (per mg microsomal protein) than the CYP2C19 activity in HLM], 51.5 for rhCYP2D6, and 8.20 for rhCYP3A4.

Panobinostat Simcyp® PBPK Model

Input parameters. The platform used for the PBPK modeling was the Simcyp® simulator (Certara Inc., Princeton, New Jersey, Version 13, release 1 or 2). Physicochemical and pharmacokinetic parameters of panobinostat used for the PBPK model are summarized in Table 2. The fraction of dose absorbed from the gastrointestinal tract (f_a) was estimated to be 1 as unchanged panobinostat in the feces of humans accounted for ≤ 3.3% of the administered dose, suggesting nearly complete oral absorption (Clive et al., 2012). The absorption rate constant (k_a) was estimated to be 0.32 per h from a population PK analysis (Savelieva et al., 2015, Supplemental Table S2b). The fu_{gut} term was entered as 1 (default). The fu_{gut} value was set to 1 in order to minimize the panobinostat F_g value and be conservative with respect to CYP3A4-mediated DDI in the intestine (*i.e.* not to under-predict the DDI). Intestinal metabolism was estimated by "top-down" modeling of the interaction of panobinostat with the CYP3A4 inhibitor, KTZ, as well as modeling the proper PK of panobinostat (*e.g.* C_{max}, AUC, concentration-time profiles) from the clinical trials used for model development (Table 3). Parameter sensitivity analysis of the panobinostat fu_{gut} value and the predicted F_g and DDI magnitude of panobinostat in the presence of KTZ are shown in Supplemental Fig. 1. The Q_{gut} term (described in Rostami-Hodjegan and Tucker 2002), which also impacts F_g, was set to be 2.8 L/h to optimize the predicted clinical PK of panobinostat and magnitude of drug interaction with KTZ. Parameter sensitivity analysis of the impact of the Q_{gut} value on panobinostat F_g and the predicted DDI magnitude of panobinostat with KTZ co-administration is shown in Supplemental Fig. 2. The minimal PBPK model within the Simcyp framework was used with a single adjusting

DMD Fast Forward. Published on September 14, 2017 as DOI: 10.1124/dmd.117.076851
This article has not been copyedited and formatted. The final version may differ from this version.

compartment. The k_{in} and k_{out} values were estimated to be 1.42 and 0.04 per h analysis (Savelieva et al., 2015, Supplemental Table S2b, as k_{24} and k_{42}). The volume of the compartment (V_{sac}) was entered as 10.5 L/kg. This value was manually optimized to predict the clinical PK of panobinostat of the trials used for model qualification. The volume of distribution (V_{ss}) was estimated to be ~13 L/kg. Panobinostat hepatic microsomal intrinsic clearance (CL_{int}) was back-calculated from the clinically observed median plasma CL of 33 L/h (Savelieva et al., 2015) using the enzyme kinetics retrograde model implemented in Simcyp. Based on an observed 1.78-fold increase in panobinostat exposure following KTZ administration in patients (Hamberg et al., 2011), the predicted fraction metabolized (fm) by CYP3A4 (fm_{CYP3A4}) was estimated as ~0.4 ($AUC_i/AUC = 1/1- fm_{CYP3A4}$]) (Shou et al., 2008). This relationship assumes complete inhibition of the CYP3A-mediated CL of panobinostat by KTZ. This value was also in-line with the results from the human ADME study where CYP-mediated oxidative CL was estimated to range from a maximum of 30-47% of the dose (Clive et al., 2012). The fm_{CYP} values for the CYP2D6 and CYP2C19 enzymes were estimated relative to CYP3A4 based upon the HLM scaled recombinant enzyme $CL_{int,u}$ values for total metabolism (Table 2). If CYP3A4 represented 40% of the total CL of panobinostat in humans, then CYP2D6 and CYP2C19 were estimated to approximately contribute 12 and 3% of the total CL, respectively. This was based upon the estimations of CYP2D6 and CYP2C19 $CL_{int,u}$ in HLM being ~3.4- and ~12-fold less than the CYP3A4 $CL_{int,u}$ value (Table 1). The *in vivo* fm_{CYP} values of CYP3A4, CYP2D6, and CYP2C19 were therefore entered as 0.4, 0.12, and 0.03 respectively. The resultant entries in the model for the individual CYP CL_{int} values and additional HLM CL calculated in Simcyp are as shown in Table 2. Panobinostat mean renal CL was entered as 3.57 L/h (Clive et al., 2012). The actual model output values of the fm or fe (fraction of elimination) for panobinostat in Simcyp

were 39, 10, 3, 34, and 14% for CYP3A4, CYP2D6, CYP2C19, additional HLM-mediated CL (representing non-CYP mediated metabolic clearance) and renal elimination, respectively. The resultant PBPK predicted values (mean, range) were: plasma CL (30 L/h, 16-57), F (0.46, 0.21-0.71), f_a (0.88, 0.39-1.0), F_g (0.68, 0.41-0.93), and F_h (0.77, 0.59-0.90).*Model development and application.* The Simcyp simulator was used for these simulations with the Simcyp "Healthy Volunteer" population. The proportion of females in the model was set as 0.5. Ten trials of 10 subjects were simulated for each dosing regimen. The input parameters for panobinostat are described in Table 2. Input values for MDZ, RIF, and KTZ (400 mg q.d.) were provided within the Simcyp simulator. The input values for these compounds can be found in the Supplemental Data (Supplemental Tables 1-3). The compound file for DEX was built "top-down" and the input parameters can be found in Supplemental Table 4. The DEX PBPK model was built to predict the PK of a single and multiple 20 mg doses of DEX (Supplemental Table 5, Supplemental Fig. 3, and Supplemental Fig. 4) and the clinical DDI with the CYP3A4/5 probe substrate triazolam (*i.e.* weak CYP3A4 induction by DEX, Supplemental Table 6). The clinical trials used to develop the model for panobinostat can be found in Table 3. The model was developed to predict the PK parameters of a dose range of 10 mg to 80 mg single and multiple Monday, Wednesday, Friday doses as well as the DDI with the CYP3A4 inhibitor, KTZ. The model was then verified to predict the weak interaction of panobinostat with DEX (Mu et al., 2016 and San-Miguel et al., 2013) then applied to predict the DDI of panobinostat with the CYP3A4 inducer, RIF and the sensitive CYP3A4/5 substrate, MDZ.

Parameter sensitivity analysis. Sensitivity analyses were performed separately and together for the panobinostat CYP3A4 inactivation parameters k_{inact} and K_I in the prediction of the MDZ AUC ratio. The range of values used in the analysis was based upon the standard

DMD Fast Forward. Published on September 14, 2017 as DOI: 10.1124/dmd.117.076851
This article has not been copyedited and formatted. The final version may differ from this version.

deviation of the experimentally determined k_{inact} and K_I values, *vide infra*. The range of k_{inact} and K_I values examined in this analysis was, therefore, 1.18-1.55 h^{-1} and 7.5-16.5 µM, respectively. Additional sensitivity analyses were performed separately for the panobinostat absorption rate constant (k_a), hepatic CYP3A4 enzyme degradation rate constant (k_{deg}) and inhibition constant (K_i) in the prediction of MDZ AUC ratio. The values used in the analysis covered an arbitrary 10-fold range of the value derived from population PK analysis (k_a 0.32 h^{-1}), literature (Obach et al 2007, CYP3A4 k_{deg} 0.0193 h^{-1}) and *in vitro* experimentation (K_i 7.5 µM). Therefore, the ranges for k_a, k_{deg}, and K_i were 0.032-3.2 h^{-1}, 0.00193-0.193 per h and 0.75-75 µM, respectively.

Data analysis. For single and multiple dose PK parameters, the C_{max} and AUC_{0-48} values are presented as the arithmetic mean with percent coefficient of variation (CV%). The T_{max} is reported as the median and range. For the DDI studies, the PK parameters are reported as geometric means and CV%. The DDI is reported as the geometric mean AUC ratio ($AUC_{inhibited\ or\ induced}/AUC_{control}$) or geometric mean C_{max} ratio ($C_{max,inhibited\ or\ induced}/C_{max,control}$) with 90% confidence intervals (CI), when the observed value was available. As a measure of model predictability, the percent prediction error (PE) was calculated as shown in Eq. 1 below. A prediction error of greater than -50% and less than +100% (predicted value within 2-fold of the observed value) for PK parameters are generally acceptable for PBPK model qualification (Sager et al., 2015). For DDI ratios, tighter criteria particularly for DDI ratios between 0.5 and 2 were followed (Guest et al. 2011).

$$Prediction\ error\ (PE) = \left(\frac{predicted\ value - observed\ value}{observed\ value}\right) \times 100 \qquad \text{Eq.1}$$

Panobinostat GastroPlus™ ACAT Model

Input parameters. A human ACAT absorption model for panobinostat was built within GastroPlus™ (Version 8.5, Simulations Plus, Inc., Lancaster, CA). The input parameters for the model are shown in Table 4. Panobinostat human PK parameters in the ACAT model were estimated from a population PK analysis using a three compartment model (Savelieva et al., 2015). The median body weight in the dataset used for the population PK analysis was 76.4 kg. Body-weight normalized CL and V_c and the values for k_{12}, k_{21}, k_{13} and k_{31} were entered in the ACAT model as described in the Supplementary Table S2b of Savelieva et al., 2015. The solubility at pH 7.6 at 37ºC was entered as 0.064 mg/ml. The first-pass elimination in the small intestine had to be defined in order to fit the ACAT model to the observed PK data. To accomplish this, an 'optimization' module was used and the first-pass elimination value in small intestine was selected for optimization. Akaike information criterion (AIC) was used to select the best fitted first-pass elimination value, and weighting was equal to $1/y^2$. Optimized first-pass elimination value in small intestine was 60%. The GastroPlus predicted first pass elimination in the liver was 26.1%. Other parameters needed for the model were as described previously (molecular weight, pKa, fu_p, B/P) and presented in Table 4.

Model application. The model was applied to predict the absorption of panobinostat with a range of stomach pH values of 0.5 to 8.0.

DMD Fast Forward. Published on September 14, 2017 as DOI: 10.1124/dmd.117.076851
This article has not been copyedited and formatted. The final version may differ from this version.

Results

In vitro CYP Inhibition

The potential for panobinostat to inhibit select CYP enzyme activities in a reversible and/or time-dependent fashion was investigated *in vitro* using pooled HLM. Panobinostat showed little to no reversible inhibition of CYP1A2, CYP2B6, CYP2C8, CYP2C9, and CYP2E1 activities and weak inhibition of CYP2C19 (IC_{50} value of ~35 µM) and CYP3A4/5 (IC_{50} values of ~7.5 µM using MDZ as the substrate and ~15 µM for testosterone). CYP2D6 was inhibited by panobinostat with an IC_{50} value of ~2 µM and K_i value of 0.167 ± 0.0286 µM (competitive inhibition). Results from pre-incubation experiments indicated that panobinostat was a time-dependent inhibitor of CYP3A4/5 and the inhibition was panobinostat concentration-dependent. The parameters associated with CYP3A4/5 time-dependent inhibition by panobinostat were (K_I and k_{inact}): 12.0 ± 4.47 µM and 1.37 ± 0.187 h^{-1}.

In vitro CYP Induction

Panobinostat was investigated for *in vitro* CYP enzyme induction potential in primary human hepatocytes of three donors. Panobinostat concentrations used in the induction study ranged from 0.01 to 1 µM (3.49 to 349 ng/ml). These concentrations spanned ~10-fold above and below the $C_{max,ss}$ concentration of the marketed 20 mg oral dose (~22 ng/ml). The positive controls used in the study included RIF (up to 10 µM), PB (1 mM), and BNF (10 µM) and the cells were treated every 24 h for 72 h. The cells were found to be viable after the induction period for the positive control inducers and panobinostat concentrations up to 0.1 µM, with a drop in cell viability of the three hepatocyte lots to ~60% compared to the vehicle control at the 1 µM concentration (data not shown). The mRNA levels of CYP1A2, CYP2B6, CYP2C9, and

CYP3A4 in human hepatocytes after treatment with panobinostat with respect to the vehicle control were all < 2-fold. Induction of CYP1A2, CYP2B6, CYP2C9, activity above 2-fold was only observed in one lot of hepatocytes (up to 2.2-, 2.6-, 2.4-fold, respectively). These induction levels were, however, less than 25% of the positive control inducers for CYP1A2 (BNF, 39-fold), CYP2B6 (PB, 12-fold), and CYP2C9 (PB, 11-fold) in that donor (Supplemental Table 7).

In vitro CYP Reaction Phenotyping

Panobinostat was found to be metabolized in HLM in the presence of co-factors for CYP (NADPH) and UGT (UDPGA) enzymes to form five metabolites: M24.2 (cyclization/hydroxylation), M34.4 (glucuronide), M37.8 (hydroxamic acid reduction), M43.5 (hydrolysis to the carboxylic acid), and M9 (an uncharacterized product), Figure 2. The identified metabolites were also found in human plasma and structures previously characterized (Clive et al., 2012). Due to the low formation of the glucuronide M34.4 in HLM, the UGT enzymes involved in formation of this product were investigated by LC-MS analysis of individual rhUGT incubations with panobinostat. Human UGT1A1, UGT1A3, UGT1A8, and UGT1A9 were found to form this metabolite with trace levels detectable in incubations with UGT1A7 and UGT2B4 (data not shown). No further kinetic evaluations were performed for this metabolite. CYP enzymes involved in formation of the other metabolites identified in HLM were investigated by incubations with individual rhCYP enzymes. Panobinostat metabolites were found in incubations with rhCYP3A4, rhCYP2D6, and rhCYP2C19. No metabolism of panobinostat was observed by radiochemical detection in incubations with any other rhCYP enzyme, including rhCYP3A5. Kinetic analysis of metabolite formation was determined in incubations with the three individual rhCYP enzymes. Representative HPLC chromatograms of the metabolites formed in the rhCYP kinetic study and the graphs of the data can be found Fig.

3A (rhCYP2C19), Fig. 3B (rhCYP2D6), and Fig. 3C (rhCYP3A4). The kinetic parameters associated with formation of individual metabolites in the rhCYP incubations can be found in Table 1 and the non-linear regression plots of the data can be found in Fig. 3D, E, and F. The predominate metabolite formed in HLM, M24.2, was formed by all three rhCYP enzymes. A di-oxygenated metabolite, not found previously in HLM, M24.2A, co-eluted with M24.2 in incubations with CYP2C19 and CYP2D6. The hydrolysis product, M43.5, was found in incubations with CYP2D6 and CYP3A4. The enzyme efficiency for formation of this metabolite by CYP2D6 was ~30-times higher than CYP3A4 (15.1 vs. 0.552 ml/h/nmol CYP), but compared to the other metabolites formed by these enzymes, and scaled contributions to total human liver microsomal CL_{int} was small (Table 1). It is likely, however, that the hydrolytic activity in plasma may also contribute to formation of M43.5 in humans *in vivo*, like that of other hydroxamic acids (Flipo et al., 2009). The hydroxamic acid reduction metabolite, M37.8, is not CYP-mediated and was found to be formed in human hepatocytes and liver slices to a more substantial level (data not shown). The relatively low levels of this metabolite in HLM, yet higher abundance in whole cell systems indicate that the reductase may reside in the cytoplasm or organelles outside of the endoplasmic reticulum.

The relative contribution of the individual CYP enzymes to the total hepatic oxidative CL of panobinostat was determined by the RAF approach. The kinetically determined V_{max} value (units of pmol/mg protein/min) of the rhCYP enzymes was scaled to human liver microsomal V_{max} by the RAF factor (ratio of the activity of substrate probe drug metabolism at substrate saturating conditions in the rhCYP vs. HLM). The scaled human liver microsomal V_{max} value and calculated $CL_{int,u}$ can be found in Table 1. The percent contribution of each of the CYPs to total oxidative hepatic microsomal $CL_{int,u}$ by the three CYP enzymes (CYP2C19, CYP2D6, and

CYP3A4) was estimated to be 6, 21, and 73%, respectively, in HLM. The relative contribution of the individual CYP enzymes to total oxidative CL_{int} in HLM determined by the RAF approach was similar to that calculated based upon CYP enzyme abundance in HLM (see Supplemental Table 8).

Panobinostat Simcyp PBPK Modeling

Simulations of panobinostat single and multiple doses. *In vitro* phenotyping studies with panobinostat found CYP3A4 primarily responsible for the oxidative metabolism of panobinostat in HLM, *vide supra*. In the human ADME study, based upon metabolites identified in the urine and feces, CYP-mediated oxidative CL was estimated to range from a maximum of 30-47% of the dose (Clive et al., 2012). Consistent with this, the contribution of CYP3A4 to the total CL of panobinostat in humans was estimated from the clinical DDI study with KTZ to be 40% (Hamberg et al., 2011). Therefore, the PBPK model was developed to incorporate 40% of the metabolic CL by CYP3A4. Based upon the relative contributions of CYP2D6 and CYP2C19 with respect to CYP3A4 determined from the kinetic study above, the contributions of these enzymes were entered as 12 and 3%, respectively. This model was used to simulate the PK of panobinostat dosed orally (15 mg to 80 mg) as a single dose or multiple Monday, Wednesday, Friday doses for 2 weeks. The simulated PK parameters were compared to those from several clinical trials (Tables 5-7). The C_{max} and T_{max} values were predicted within ~2-fold of the observed value for both single and multiple doses. The AUC was also predicted within 2-fold for most trials with the exception of the 60 and 80 mg doses in trial B2102, where the exposure was over-predicted (prediction errors of +150 and +183%, respectively), Table 6. The variability (CV%) of the AUC values were predicted relatively well, however the variability in the C_{max} values were over-predicted compared to the observed values. The variability in C_{max} was most

sensitive to the CV% entered for V_{ss} (15%), see Table 2. Evaluation of changes of the default CV% (30%) for absorption parameters (f_a, k_a, Q_{gut}) or intrinsic clearance did not impact the variability in panobinostat C_{max} (20 mg single dose evaluated, *data not shown*). A reduction in the V_{ss} CV% from 15 to 8% resulted in a CV% value closer to the actual variability in C_{max} (predicted 67% vs. actual 57-61% for the 20 mg single dose) as well as the CV% for AUC (predicted 54% vs. actual 48-58%), *data not shown*. Representative concentration-time profiles of panobinostat after single and multiple 20 mg doses in patients are shown in Fig. 4.

Simulation of the drug interaction of panobinostat with KTZ. The PBPK model was also built to capture the clinical DDI magnitude of the strong CYP3A4 inhibitor, KTZ. The model predicted the PK parameters of panobinostat (C_{max} and AUC) in the absence or presence of KTZ within 2-fold of the actual values (Table 7). The geometric mean C_{max} and AUC ratios were also predicted well. The predicted and observed geometric mean C_{max} ratios were 1.7 and 1.6, respectively, and the AUC ratios were both 1.8. The concentration-time profiles of panobinostat in the absence and presence of KTZ is shown in Fig 5.

Simulation of the drug interaction of panobinostat with DEX. The PBPK model was verified to predict the weak interaction of DEX with panobinostat. The model input parameters and verification results for modeling DEX PK (20 mg single and multiple doses) and the weak clinical CYP3A4 induction with triazolam can be found in the Supplemental Data. The results of the prediction of the interaction of DEX (20 mg) with panobinostat (20 mg Monday, Wednesday, Friday doses) are shown in Table 8. The predicted PK parameters were within two-fold of the actual values and the AUC and C_{max} ratios were within the acceptable prediction criteria as described in Guest et al. (2011).

Prediction of panobinostat PK in the presence of RIF. The model was then applied to predict the drug interaction of panobinostat with a strong CYP3A4 inducer, RIF, *in lieu* of an actual clinical trial. RIF (600 mg) was dosed once a day for 14 days and a single dose of panobinostat (20 mg) was given on day 7. The results of the prediction are shown in Table 9 and the concentration-time profiles of panobinostat and RIF are shown in Fig. 6. The predicted geometric mean C_{max} and AUC ratios were 0.45 (55% decrease in C_{max}) and 0.35 (65% decrease in AUC), respectively. This original modeling was performed using Simcyp, version 13, where the RIF Ind_{max} value (fold change with respect to the vehicle control) for CYP3A4 was 8 versus 16 in later versions of the software. A parameter sensitivity analysis of the RIF Ind_{max} parameter on panobinostat AUC ratio (using the Simcyp population representative) can be found in Supplemental Fig. 5. The predicted AUC ratio ranged from 0.32 to 0.14 (68% to 86% reduction in AUC) with RIF Ind_{max} values of 8 to 16.

Prediction of MDZ PK in the presence of panobinostat. Due to the *in vitro* CYP3A4 reversible and time-dependent inhibition properties of panobinostat, the drug-interaction of panobinostat with the sensitive CYP3A4/5 substrate, MDZ, was predicted. Panobinostat (20 mg) was dosed orally on Monday, Wednesday, and Friday for 2 weeks and a single 5 mg dose of MDZ was given on day 15 with the last dose of panobinostat. The results of the simulation are found in Table 10 and the concentration-time profiles of MDZ and panobinostat are shown in Fig 7. The predicted geometric mean C_{max} and AUC ratios were both 1.04.

Sensitivity analysis of select panobinostat PBPK model input parameters on the MDZ AUC ratio. The design of the panobinostat-MDZ trial simulation is as described in the section above. The range of the parameter values chosen for the sensitivity analysis are described in the Materials and Methods section and encompassed the standard deviation of experimentally

determined CYP3A4 time-dependent inactivation parameters for panaobinostat (k_{inact}, K_I) or an arbitrary 10-fold range (panobinostat k_a, hepatic CYP3A4 k_{deg}, and panobinostat K_i for CYP3A4 reversible inhibition). The results of the sensitivity analysis can be found in Fig. 8. Variation of the K_I or k_{inact} value separately (Fig. 8A and Fig. 8B) or together (Fig. 8C) was not impactful to the MDZ AUC ratio (AUC ratio <1.1). The panobinostat k_a value or CYP3A4 hepatic k_{deg} value (Fig. 8D and Fig. 8F) was also not sensitive to the DDI effect on MDZ. A reduction in the K_i value for CYP3A4 to 0.75 μM (10 times lower than actual) increased the AUC ratio to slightly over 1.1.

Panobinostat GastroPlus ACAT Modeling

Using the established ACAT absorption model for panobinostat in humans, the PK profiles following a single oral dose of 20, 30 and 40 mg panobinostat were simulated. The observed and predicted PK parameters of each simulation are summarized in Table 5 (values in parentheses). The projected panobinostat absorption in humans was ~100% within the dose range of 20 - 40 mg. The predicted T_{max}, C_{max} and $AUC_{0\text{-}48h}$ were similar to the corresponding observed values. The similarity between the observed and the projected PK profiles and parameters suggested that ACAT absorption model for panobinostat was qualified. Sensitivity analysis on the stomach pH ranging from 0.5 to 8.0 was therefore performed. Fig. 9 presents the absorption of 20 mg panobinostat under the stomach pH in a range of 0.5 – 8.0. The predicted absorption was ~100% for this range of pH values.

Discussion

The use of PBPK modeling in drug development and ultimately in regulatory submissions has become increasingly apparent from the literature and recent product labels (Zhao et al., 2011, 2012; Huang and Rowland, 2012; Huang et al., 2013; Jones et al., 2015; Jamei 2016). PBPK models are particularly important for evaluating potential consequences of intrinsic (e.g. human physiology, genetics, etc.) and extrinsic factors (e.g. co-administration of other drugs) on the exposure of the drug in different tissues, organs, and in the systemic circulation. With well qualified PBPK models for the intended modeling purpose, predictions can be made for untested or difficult-to-test clinical scenarios and can be particularly useful for dosing recommendations. Particularly in the case of Farydak®, it was undesirable to expose patients to sub-therapeutic levels of panobinostat as would occur in the presence of strong CYP3A4 inducers. Therefore, the PBPK modeling and simulation work presented here was influential for the dosing strategy with respect to co-administration of panobinostat with strong CYP3A4 inducers as well as sensitive substrates of CYP3A4/5 *in lieu* of actual clinical trials.

Results from the *in vitro* assays presented here found panobinostat not likely to be a clinical inducer of major drug metabolizing CYP enzymes, however, was found to be a reversible *in vitro* inhibitor of CYP2D6 and a weaker inhibitor of CYP3A4/5 and CYP2C19. A clinical DDI study investigating the potential magnitude of effect of panobinostat on the CYP2D6 substrate, dextromethorphan, was therefore run and reported in Feld et al., 2013. Panobinostat (20 mg dosed every other day for 3 days) increased dextromethorphan exposure by 64%, indicating that panobinostat is a weak CYP2D6 inhibitor *in vivo*. The observed mean panobinostat C_{max} value in the clinical DDI study was 25.8 ng/ml (0.074 µM). As mentioned in the previous manuscript, based on the empirical equation, $1+[I]/K_i$, the AUC ratio was predicted

to be 1.4, therefore a clinical inhibition of CYP2D6 by panobinostat was expected in this study (Feld et al., 2013). Since the initiation of this clinical DDI trial, regulatory guidance has described the use of more mechanistic models, including PBPK, rather than empirical methods, to assess the risk of drug interaction potential and decisions regarding whether clinical DDI studies may be warranted (FDA 2012, EMA 2012). These types of models, which incorporate time-varying concentrations of both the perpetrator and victim drug and time-dependent effects of CYP inhibition and induction, offer better prediction outcomes (Einolf 2007).

A PBPK model for panobinostat was developed to describe single and multiple (Monday, Wednesday, Friday) dose PK and the magnitude of drug interaction with KTZ. The model incorporated the reversible and time-dependent CYP inhibition properties of panobinostat as well as the relative contributions of CYP3A4, CYP2D6, and CYP2C19 to the total oxidative CL of panobinostat in humans. The relative contributions of these individual CYP enzymes in humans were determined by both *in vitro* scaling of rhCYP kinetic data as well as scaling 'top-down' using the results of the KTZ DDI study (which defined the approximate contribution of CYP3A4). The relative contributions of the individual CYP enzymes determined *in vitro* were scaled to humans *in vivo* based upon the ~40% contribution of CYP3A4 to panobinostat CL in humans determined from the KTZ DDI study (Hamberg et al., 2011) with confirmation of the extent of CYP-mediated oxidative metabolism from the human ADME study (Clive et al., 2012). The resultant contributions of CYP3A4, CYP2D6, and CYP2C19 to the total *in vivo* CL panobinostat were estimated to be 40, 12, and 3%, respectively. Additional CL pathways in humans, such as reduction, hydrolysis, and glucuronidation, were grouped together in the model to equate to the remainder of total panobinostat CL.

This PBPK model appropriately predicted the PK parameters of panobinostat over the dose range of 10-80 mg, with most parameters predicted within 2-fold of the actual value. In the single dose trials (Table 5, Fig. 4A), the model predicted the C_{max} and $AUC_{0\text{-}48h}$ values within a prediction error of -33 to +24 and -35 to +57%, respectively. In the multiple dose study (Table 6, Fig. 4B), for trials B2101 and B2102 the prediction error was within 2-fold for C_{max} at all doses and AUC up to the 40 mg dose. A higher prediction error was seen with the prediction of AUC at higher doses (60 and 80 mg) in trial B2102 (prediction error of +150 and +183%).

Importantly, this PBPK model was able to simulate the clinical DDI of panobinostat (C_{max} and AUC ratios) with KTZ, which established the contribution of CYP3A4 to total panobinostat CL in the model (Table 7, Fig. 5). The relative contribution of the other CYP enzymes, *i.e.* CYP2D6 and CYP2C19, remain to be verified clinically, however, their contributions are expected to be low and likely do not warrant any further investigation as complete inhibition of one of these enzymes is not expected to increase panobinostat exposure by more than ~14%. The interindividual variability in CL was reported to be higher, 74% (Savelieva et al., 2015).

With the verification of the PBPK model to predict panobinostat PK and DDI with KTZ and DEX, the effect of multiple 600 mg QD doses of RIF on panobinostat PK was predicted. Based upon the results of the PBPK modeling, co-administration with strong inducers of CYP3A4 are to be avoided when taking Farydak®, due to the predicted (at least) 65% reduction in exposure (Table 9, Fig. 6). The reference to this modeling and simulation data in support of the labeling recommendation is present in the FDA-approved product label (Farydak® prescribing information, 2016). PBPK modeling is particularly useful in cases like this, where there is no benefit to patients, especially cancer patients, exposed to sub-therapeutic levels of an

DMD Fast Forward. Published on September 14, 2017 as DOI: 10.1124/dmd.117.076851
This article has not been copyedited and formatted. The final version may differ from this version.

investigational drug when mechanistically evaluating the effect of a strong inducer. Particularly for RIF, PBPK modeling has been found to be predictive of drug interactions with respect to CYP3A4 induction especially if the fm_{CYP3A4} for the victim drug clearance has been defined appropriately (Wagner et al., 2016, Almond et al., 2016). If the role of CYP3A4 for the victim drug has been properly defined by *in vitro* and *in vivo* methods (*e.g.* clinical inhibition with a strong CYP3A4 inhibitor), then modeling and simulation can be used to predict the effect of induction with qualified inducer models.

Particularly in the case of time-dependent CYP3A4 inhibition, modeling time-dependent effects, such as time-varying concentrations of perpetrator in the liver and intestine as well as the actual clinical dosing regimen (*e.g.* Monday, Wednesday, Friday dosing) are important to capture in the prediction model. Based upon the PBPK modeling, panobinostat is expected to increase the exposure (AUC) of the sensitive CYP3A4 substrate, MDZ by only 1.04-fold (Table 10, Fig. 7), *i.e.* <10%, as stated in the FDA Farydak® product label (Farydak® FDA prescribing information, 2016). This implies that there will be little, if any, effect of panobinostat when co-administered with CYP3A4/5-cleared substrates. In contrast, the EMA product label (Farydak® EMA Summary of Product Characteristics) or Farydak® EMA Risk Management Plan (2015) do not mention PBPK modeling results for panobinostat with sensitive CYP3A4/5 substrates. Although, the modeling is acknowledged in the Farydak® EMA Assessment Report (2015), it did not appear to influence the EMA product label.

Though panobinostat has pH-dependent solubility, overall more than 16 mg of drug substance can be fully dissolved in a pH range of 1.2 -7.6. Given its high permeability, relatively good solubility and low dose level (20 mg), the PBPK model predicts that elevated gastric pH would not impact panobinostat absorption in humans (Fig. 9). This implies that co-

administration with agents that increase the pH in the stomach (antacids, H_2 receptor antagonists, and proton-pump inhibitors) is not likely to affect the exposure of panobinostat in patients. It is noteworthy that the potential prolongation on gastrointestinal (GI) transit time by proton pump inhibitors (Rasmussen et al., 1997) is not considered in the panobinostat ACAT model. Fig. 9 shows complete absorption of a 20 mg panobinostat in humans, suggesting that further increase on GI transit time would not result in higher absorption. The simulation result is presented in Farydak® drug label (Farydak® prescribing information, 2016) *in lieu* of clinical study. In a recent publication, results of GastroPlus modeling found a signification correlation of model predicted AUC and C_{max} ratios with clinical DDI observations of compounds known to have pH-dependent DDI (Zhu et al., 2016). Recently, an alectinib GastroPlus ACAT model predicted that gastric pH changes would not affect alectinib exposure and the absorption modeling was included in the new drug application to FDA to successfully replace clinical assessment study (Parrott et al, 2016).

In conclusion, PBPK models were developed to predict the DDI of panobinostat as a victim and perpetrator of CYP3A4, as well as pH-dependent DDI. This modeling was incorporated into the FDA-approved product label for Farydak®, providing information to aid in dosing recommendations for co-administration with other drugs. This work exemplifies how PBPK modeling can improve efficiency in clinical drug development, aiding in the decisions whether dedicated mechanistic clinical DDI trials are necessary, particularly in consideration of the well-being of patients.

Acknowledgments

The authors would like to thank the following colleagues from Novartis (East Hanover, NJ): Grazyna Ciszewska, Lawrence Jones, Amy Wu, and Tapan Ray for the synthesis of [^{14}C]panobinostat and Mu Song from Oncology Clinical Pharmacology, for his advice and support of this work.

Authorship Contributions

Participated in research design: Einolf, Lin, Won, Gu, He, Mangold

Conducted experiments: Einolf, Lin, Won, Wang, Chun, Gu

Performed data analysis: Einolf, Lin, Won, Wang, Chun, Gu, He, Mangold

Wrote or contributed to the writing of the manuscript: Einolf, Lin

References

Almond LM, Mukadam S, Gardner I, et al. (2016) Prediction of drug-drug interactions arising from CYP3A induction using a physiologically based dynamic model. *Drug Metab Dispos* 44:821-32.

Cheng T, Grasse L, Shah J, Chandra J (2015) Panobinostat, a pan-histone deacetylase inhibitor: rationale for and application to treatment of multiple myeloma. *Drugs Today* 51:491-504.

Clive S, Woo MM, Nydam T, Kelly L, Squier M, and Kagan M (2012) Characterizing the disposition, metabolism, and excretion of an orally active pan-deacetylase inhibitor, panobinostat, via trace radiolabeled 14C material in advanced cancer patients. *Cancer Chemother Pharmacol* 70:513-22.

DeAngelo DJ, Spencer A, Bhalla KN, et al. (2013) Phase Ia/II, two-arm, open-label, dose-escalation study of oral panobinostat administered via two dosing schedules in patients with advanced hematologic malignancies. *Leukemia* 27:1628-36.

Einolf HJ (2007) Comparison of different approaches to predict metabolic drug-drug interactions. *Xenobiotica* 37:1257-1294.

EMA (2012) Guideline on the investigation of drug interactions. European Medicines Agency. June 2012.

http://www.ema.europa.eu/docs/en_GB/document_library/Scientific_guideline/2012/07/WC500129606.pdf

Farydak® EMA Assessment Report (2015)

http://www.ema.europa.eu/docs/en_GB/document_library/EPAR_-_Public_assessment_report/human/003725/WC500193300.pdf

Farydak® EMA Risk Management Plan (2015)

http://www.ema.europa.eu/docs/en_GB/document_library/EPAR_-_Risk-management-plan_summary/human/003725/WC500188847.pdf

Farydak® EMA Summary of Product Characteristics

http://www.ema.europa.eu/docs/en_GB/document_library/EPAR_-_Product_Information/human/003725/WC500193298.pdf

Farydak® FDA prescribing information (2016), June 2016

https://www.pharma.us.novartis.com/sites/www.pharma.us.novartis.com/files/farydak.pdf

FDA Clin Pharm Rev (2015) FDA Center for Drug Evaluation and Research Clinical Pharmacology and Biopharmaceutics Review(s) of Farydak® (panobinostat) http://www.accessdata.fda.gov/drugsatfda_docs/nda/2015/205353Orig1s000ClinPharmR.pdf

FDA (2012) Draft Guidance for Industry, Drug Interaction Studies-Study Design, Data Analysis, Implicationsfor Dosing, and Labeling Recommendations. U.S. Department of Health and Human Services Food and Drug Administration, Center for Drug Evaluation and Research (CDER). February 2012.

http://www.fda.gov/downloads/drugs/guidancecomplianceregulatoryinformation/guidances/ucm292362.pdf

Feld R, Woo MM, Leigh N, et al., (2013) A clinical investigation of inhibitory effect of panobinostat on CYP2D6 substrate in patients with advanced cancer. *Cancer Chemother Pharmacol*; 72:747-55.

Flarakos J, Du Y, Bedman T, et al., (2016) Disposition and metabolism of [^{14}C] Sacubitril/Valsartan (formerly LCZ696) an angiotensin receptor neprilysin inhibitor, in healthy subjects. *Xenobiotica* 46:986-1000.

Flipo M, Charton J, Hocine A, Dassonneville S, Deprez B, and Deprez-Poulain R (2009) Hydroxamates: Relationships between structure and plasma stability. *J Med Chem* 52:6790-6802.

Fukutomi A, Hatake K, Matsui K, Sakajiri S, Hirashima T, Tanii H, Kobayashi K, and Yamamoto N (2012) A phase I study of oral panobinostat (LBH589) in Japanese patients with advanced solid tumors. *Invest New Drugs* 30:1096-106.

Garnock-Jones KP (2015) Panobinostat: first global approval. *Drugs* 75:695-704.

Guest EJ, Aarons L, Houston JB, Rostami-Hodjegan A, Galetin A (2011) Critique of the two-fold measure of prediction success for ratios: application for the assessment of drug-drug interactions. *Drug Metab Dispos* 39:170-3.

Hamberg P, Woo MM, Chen LC, et al. (2011) Effect of ketoconazole-mediated CYP3A4 inhibition on clinical pharmacokinetics of panobinostat (LBH589), an orally active histone deacetylase inhibitor. *Cancer Chemother Pharmacol* 68:805-13.

Huang SM, Abernethy DR,Wang Y, Zhao P, and Zineh I (2013) The utility of modeling and simulation in drug development and regulatory review. *J Pharm Sci* 102: 2912–2923.

Huang SM and Rowland M (2012) The role of physiologically based pharmacokinetic modeling in regulatory review. *Clin Pharmacol Ther* 91: 542–549.

Jamei M (2016) Recent Advances in Development and Application of Physiologically-Based Pharmacokinetic (PBPK) Models: a Transition from Academic Curiosity to Regulatory Acceptance. *Curr Pharmacol Rep* 2: 161-169.

Jones HM, Chen Y, Gibson C, Heimbach T, Parrott N, Peters SA, Snoeys J, Upreti VV, Zheng M, Hall SD (2015) Physiologically based pharmacokinetic modeling in drug discovery and development: a pharmaceutical industry perspective. *Clin Pharmacol Ther* 97:247-62.

Mu S, Kuroda Y, Shibayama H, Hino M, Tajima T, Corrado C, Lin R, Waldron E, Binlich F, Suzuki K (2016) Panobinostat PK/PD profile in combination with bortezomib and dexamethasone in patients with relapsed and relapsed/refractory multiple myeloma. *Eur J Clin Pharmacol* 72:153-61.

Obach RS, Walsky RL, and Venkatakrishnan K (2007) Mechanism-based inactivation of human cytochrome p450 enzymes and the prediction of drug-drug interactions. *Drug Metab Dispos* 35:246-55.

Parrott NJ, Yu LJ, Takano R, Nakamura M, Morcos PN (2016) Physiologically Based Absorption Modeling to Explore the Impact of Food and Gastric pH Changes on the Pharmacokinetics of Alectinib. *AAPS J* 18:1464-1474.

Rasmussen L, Qvist N, Oster-Jørgensen E, Rehfeld JF, Holst JJ, Pedersen SA (1997) A double-blind placebo-controlled study on the effects of omeprazole on gut hormone secretion and gastric emptying rate. *Scand J Gastroenterol* 32:900-5.

Rostami-Hodjegan A and Tucker GT (2002) The effects of portal shunts on intestinal cytochrome P450 3A activity. *Hepatology* 35:1549-50.

Sager JE, Yu J, Ragueneau-Majlessi I, Isoherranen N (2015) Physiologically Based Pharmacokinetic (PBPK) Modeling and Simulation Approaches: A Systematic Review of Published Models, Applications, and Model Verification. *Drug Metab Dispos*; 43:1823-37.

San-Miguel JF, Richardson PG, Günther A, et al. (2013) Phase Ib study of panobinostat and bortezomib in relapsed or relapsed and refractory multiple myeloma. *J Clin Oncol*; 31(29):3696-703.

Savelieva M, Woo MM, Schran H, Mu S, Nedelman J, and Capdeville R (2015) Population pharmacokinetics of intravenous and oral panobinostat in patients with hematologic and solid tumors. *Eur J Clin Pharmacol* 71:663-72.

Shapiro GI, Frank R, Dandamudi UB, et al. (2012) The effect of food on the bioavailability of panobinostat, an orally active pan-histone deacetylase inhibitor, in patients with advanced cancer. *Cancer Chemother Pharmacol* 69:555-62.

Shou M, Hayashi M, Pan Y, Xu Y, Morrissey K, Xu L, Skiles GL (2008) Modeling, prediction, and in vitro in vivo correlation of CYP3A4 induction. *Drug Metab Dispos* 36:2355-70.

Wagner C, Pan Y, Hsu V, Sinha V, and Zhao P (2016) Predicting the effect of CYP3A inducers on the pharmacokinetics of substrate drugs using physiologically based pharmacokinetic (PBPK) modeling: An analysis of PBPK submissions to the US FDA. *Clin Pharmacokinet* 55:475-83.

Wahaib K, Beggs AE, Campbell H, Kodali L, Ford PD (2016). Panobinostat: A histone deacetylase inhibitor for the treatment of relapsed or refractory multiple myeloma. *Am J Health Syst Pharm* 73:441-50.

Zhao P, Rowland M, and Huang SM (2012) Best practice in the use of physiologically based pharmacokinetic modeling and simulation to address clinical pharmacology regulatory questions. *Clin Pharmacol Ther* 92: 17–20.

Zhao P, Zhang L, Grillo JA, et al., (2011) Applications of physiologically based pharmacokinetic (PBPK) modeling and simulation during regulatory review. *Clin Pharmacol Ther*; 89: 259–267.

Zhu AZ, Ho MD, Gemski CK, Chuang BC, Liao M, and Xia CQ (2016) Utilizing In Vitro Dissolution-Permeation Chamber for the Quantitative Prediction of pH-Dependent Drug-Drug Interactions with Acid-Reducing Agents: a Comparison with Physiologically Based Pharmacokinetic Modeling. *AAPS J* 18:1512-1523.

DMD Fast Forward. Published on September 14, 2017 as DOI: 10.1124/dmd.117.076851
This article has not been copyedited and formatted. The final version may differ from this version.

Figure Legends

Fig. 1. The chemical structure of panobinostat.

Fig. 2. Metabolism of panobinostat in HLM. (A) HPLC chromatographic profiles of [^{14}C]panobinostat incubated with HLM in the absence (A) or presence (B) of the co-factors for CYP- and UGT-enzyme mediated metabolism, NADPH and UDPGA, respectively.

Fig. 3. Kinetics of panobinostat metabolism by rhCYP2C19, rhCYP2D6, and rhCYP3A4. Representative HPLC chromatographic profile from the kinetic analysis of [^{14}C]panobinostat metabolism in incubations with (A) rhCYP2C19 (17 µM sample), (B) rhCYP2D6 (4 µM sample), and (C) rhCYP3A4 (49 µM sample) are shown. The "I" indicates an impurity that was ≤ 7% of the total radioactivity. The average rate of metabolite formation of duplicate samples from (D) rhCYP2C19, (E) rhCYP2D6, and (F) rhCYP3A4 incubations were plotted against the panobinostat concentration. The solid line represents a non-linear regression of the data used to determine the kinetic parameters and the error bars indicate the range of the duplicate samples.

Fig. 4. Observed and predicted concentration-time profiles of a (A) single 20 mg oral dose of panobinostat or (B) multiple 20 mg oral doses (Monday, Wednesday, Friday) of panobinostat for 2 weeks. The solid black line represents the simulated concentration-time profiles of panobinostat and the dotted lines are the 5th and 95th confidence intervals. The points on the graph are the observed mean concentration-time data from trial CLBH589B2101 (squares) and CLBH589B2102 (circles) ± standard deviation (error bars).

Fig. 5. Observed and predicted concentration-time profiles of panobinostat in the absence or presence of KTZ. KTZ (400 mg) was dosed once a day for 5 days. One hour after the 3rd dose of KTZ, 20 mg panobinostat was administered and concentrations of panobinostat were

measured up to 48h. The solid black and grey lines represent the simulated mean concentration-time profiles of panobinostat in the absence and presence of KTZ, respectively. The corresponding dotted lines are the predicted 10^{th} and 90^{th} confidence intervals. The data points on the graphs are the observed mean ± standard deviation (error bars) of panobinostat plasma concentrations (Hamberg et al., 2011).

Fig. 6. Predicted concentration-time profile of panobinostat in the presence or absence of RIF. (A) The lines represent the simulated mean concentration-time profile of panobinostat (20 mg single dose on day 7) in the absence (black line) or presence (grey line) of RIF. (B) The solid black line represents the simulated mean concentration-time profile of RIF (600 mg QD for 14 days).

Fig. 7. Predicted concentration-time profile of MDZ in the presence or absence of panobinostat. (A) The lines represent the mean simulated concentration-time profile of MDZ (5 mg single dose on day 15) in the absence (black line) or presence (grey line) of panobinostat. (B) The solid black line represents the simulated concentration-time profile of panobinostat (20 mg oral dosed weekly on Monday, Wednesday, Friday).

Fig. 8. Sensitivity analysis of panobinostat inactivation parameters for CYP3A4 (A) K_I , (B) k_{inact}, or (C) both K_I and k_{inact} , (D) CYP3A4 k_{deg} value, (E) the reversible CYP3A4 inhibition constant, K_i, and (F) the panobinostat k_a value on the predicted AUC ratio of MDZ in the presence of panobinostat.

Fig. 9. PBPK model projected absorption of panobinostat (20 mg) versus stomach pH in humans.

Tables

TABLE 1

Kinetic parameters for panobinostat metabolism by recombinant human CYP2C19, CYP2D6, and CYP3A4

				Enzyme efficiency	**Estimation of individual CYP contributions to total human liver microsomal oxidative CL_{int} of panobinostat**		
CYP	**Metabolite**	$K_{m,u}$ *µM*	V_{max} h^{-1}	$V_{max}/K_{m,u}$ *ml/h/nmol CYP*	**Scaled V_{max}**[a] *nmol/h/mg protein*	**Scaled $CL_{int,u}$** *ml/h/mg protein*	**% contribution**[d]
CYP2C19	Total[b]	6.41 ± 0.40	118 ± 1.7 (14.7)[c]	18.4	0.299	0.0466	6
	M9	10.8 ± 2.0	6.35 ± 0.46 (0.792)	0.588	0.0161	0.00149	
	M24.2 + M24.2A	7.93 ± 0.43	120 ± 1.7 (15.1)	15.1	0.308	0.0388	
CYP2D6	Total	0.554 ± 0.043	48.3 ± 0.74 (4.97)	87.2	0.0965	0.174	21
	M9	10.3 ± 5.0	2.72 ± 0.56 (0.281)	0.264	0.00546	0.000530	
	M24.2 + M24.2A	0.536 ± 0.048	40.2 ± 0.71 (4.14)	75.0	0.0804	0.150	
	M43.5	0.424 ± 0.042	6.41 ± 0.12 (0.661)	15.1	0.0128	0.0303	
CYP3A4	Total	8.98 ± 0.44	226 ± 2.7 (44.4)	25.1	5.41	0.603	73
	M9	14.2 ± 0.99	56.8 ± 1.1 (11.1)	4.00	1.35	0.0953	
	M24.2	7.49 ± 0.58	160 ± 2.8 (31.4)	21.3	3.83	0.512	
	M43.5	21.0 ± 1.9	11.6 ± 0.35 (2.28)	0.552	0.278	0.0132	

$K_{m,u}$, unbound K_m (corrected for the unbound fraction in the microsomes, fu_{mic}). The fu_{mic} was 1.0 for the rhCYP2C19 and rhCYP2D6 incubations (0.20 and 0.24 mg protein/ ml, respectively) and 0.99 for the rhCYP3A4 incubations (0.26 mg protein / ml), determined by ultracentrifugation (data not shown).

[a]Scaled V_{max} is an estimate of the V_{max} for that CYP enzyme in HLM. It was calculated by dividing the V_{max} value in parentheses (units of nmol/h/mg microsomal protein) from the rhCYP enzyme by the RAF values: 49.1 (CYP2C19), 51.5 (CYP2D6), 8.20 (CYP3A4), see Materials and Methods Section

[b]Total metabolism

[c]the value in parentheses is the V_{max} value with the units of nmol/h/mg microsomal protein

[d]The % contribution of the individual CYP enzyme to total panobinostat oxidative $CL_{int,u}$ in HLM = individual CYP $CL_{int,u} \div \Sigma$ CYP $CL_{int,u}$ x 100

DMD Fast Forward. Published on September 14, 2017 as DOI: 10.1124/dmd.117.076851
This article has not been copyedited and formatted. The final version may differ from this version.

TABLE 2

Simcyp model input parameters for panobinostat

Parameter (unit)	Value	Source
Physical Chemistry and blood binding		
Molecular weight (g/mol)	349.44	
logP	2.643	Calculated LogP (in-house)
Compound type	Diprotic acid	
pK_a	8.4 and 9	Measured (internal data)
B/P	1.4	Measured (internal data)
$f_{u,plasma}$	0.104	Measured (internal data)
Absorption		
Model used	1st order	
f_a (CV%)	1 (30%, default)	Clive et al., 2012
k_a, per h (CV%)	0.32 (30%, default)	Savelieva et al., 2015
fu_{gut}	1	Simcyp default and to minimize F_g value
Q_{gut}, L/h (CV%)	2.8 (30%, default)	Manually optimized for fit of clinical PK and DDI data
Distribution		
Model used	Minimal PBPK	
k_{in}, per h	1.42	Savelieva et al., 2015
k_{out}, per h	0.04	Savelieva et al., 2015
V_{sac}, L/kg	10.5	Manually optimized for fit of clinical PK data
V_{ss}, L/kg (CV%)	13 (15%)	Estimate
Elimination		
Model used	Retrograde model[a]	
CL_{int} CYP3A4, µl/min/pmol CYP	0.3071	Based upon relative CYP contributions determined in vitro
CL_{int} CYP2D6, µl/min/pmol CYP	1.578	
CL_{int} CYP2C19, µl/min/pmol CYP	0.2254	
Additional HLM CL, µl/min/mg protein (CV%)	35.96 (30%, default)	Estimate of non-CYP mediated CL
CL_R, L/h (CV%)	3.57 (30%, default)	Clive et al., 2012
Interaction		
K_i, CYP2C19 (µM)	17.5[b]	Measured
K_i, CYP2D6 (µM)	0.167	Measured
K_i, CYP3A4 (µM)	7.5[b]	Measured
k_{inact} (per h)	1.37 ± 0.187	Measured
K_I (µM)	12.0 ± 4.47	Measured

B/P, blood to plasma ratio
[a]The CYP CL_{int} and additional HLM CL was estimated using the Simcyp retrograde model, see Materials and Methods
[b]$IC_{50}/2$

DMD Fast Forward. Published on September 14, 2017 as DOI: 10.1124/dmd.117.076851
This article has not been copyedited and formatted. The final version may differ from this version.

TABLE 3

Simulated Trials

Type of simulation	Trial description	Reference
Model development		
	Study CLBH589B2101: A phase IA, 2-arm, multicenter, dose-escalation study of panobinostat administered orally on two dose schedules in adult patients with advanced solid tumors or non-Hodgkin's lymphoma	FDA Clin Pharm Rev, 2015
	Study CLBH589B2102: Phase IA/II, two-arm, open-label, dose-escalation study of oral panobinostat administered via two dosing schedules with advanced hematologic malignancies	De Angelo et al., 2013 FDA Clin Pharm Rev, 2015
	Study CLBH589B2110: Effect of KTZ-mediated CYP3A4 inhibition on clinical PK of panobinostat in patients	Hamberg et al., 2011 FDA Clin Pharm Rev, 2015
Model verification	Study CLBH589B2207: Phase Ib study of panobinostat and bortezomib in relapsed or relapsed and refractory multiple myeloma (exposure of panobinostat in combination with DEX)	San-Miguel et al., 2013 and Mu et al., 2016
Model application		
	Simulated effect of RIF (600 mg QD) dosed for 14 days on the PK of panobinostat (20 mg single dose) on day 7	
	Simulated effect of panobinostat (20 mg) dosed orally on Monday, Wednesday, Friday for 2 weeks on the PK of MDZ (5 mg single dose) on day 15	

TABLE 4

GastroPlus ACAT model input parameters for panobinostat

Parameter (unit)	**Value**
Dosage form	Immediate release tablet[a]
logP[b]	2.8
Solubility (mg/ml)	0.064 at pH 7.6
pKa	8.4
Dose volume (ml)	250
Particle density (g/ml)[b]	1.2
Mean particle radius (μm) (standard deviation[b])	15 (0)
Particle radius bin	1
Precipitation time (sec)[b]	900
Diffusion coefficient (cm^2/sec x 10^5)[b]	0.43
Permeability (cm/s x 10^4)	2.289
Simulation time (h)	48
Body weight (kg)	69.1 (20 mg) 67.8 (30 mg) 79.1 (40 mg)
First pass elimination in small intestine, %	60
First pass elimination in liver, %	26.1
CL (L/h/kg)[c]	0.433
V_c (L/kg)[c]	0.325
k_{12} (per h)[c]	1.81
k_{21} (per h)[c]	0.507
k_{13} (per h)[c]	1.42
k_{31} (per h)[c]	0.04

[a]Dosage forms selected in GastroPlus™ for simulations
[b]Predicted by ADMET predictor or default values in GastroPlus™
[c]Population PK analysis of human intravenous data

TABLE 5

Clinically observed and Simcyp [and GastroPlus] model-predicted pharmacokinetic parameters of panobinostat after a single oral dose.

PK parameter	**Study**	**Dose**					
		15 mg	**20 mg**	**30 mg**	**40 mg**	**60 mg**	**80 mg**
N	B2101	3	36	31		4	
	B2102		9	18	24	53	18
	Simulated	*100*	*100*	*100*	*100*	*100*	*100*
C_{max} *ng/ml*	B2101	12.2 (65)	23.6 (57)	34.0 (56)		55.4 (40)	
	B2102		19.5 (61)	39.8 (69)	58 (59)	66.9 (70)	63.5 (58)
	Simulated	*14.6 (146)*	*19.5 (146) [31][a]*	*29.2 (146) [47.5]*	*39.1 (146) [58.9]*	*58.8 (146)*	*78.7 (146)*
	PE (%)[b]	*+20*	*0 to -17 [+31 to +59]*	*-27 to -14 [+19 to +40]*	*-33 [+2]*	*-12 to +6*	*+24*
AUC_{0-48} *ng × h/ml*	B2101	n/a	198 (48)	262 (49)		390 (28)	
	B2102		131 (58)	310 (117)	299 (76)	330 (62)	342 (54)
	Simulated	*96.5 (87)*	*129 (87) [151]*	*195 (88) [231]*	*262 (88) [280]*	*398 (88)*	*538 (89)*
	PE (%)		*-2 to -35 [-24 to +15]*	*-37 to -26 [-25 to -12]*	*-12 [-6]*	*+2 to +21*	*+57*
T_{max}[c] *h*	B2101	1 (0.5-2)	1 (0.5-4.5)	1 (0.5-8)			
	B2102		2.1 (0.5-3.1)	1 (0.5-28)	0.8 (0.5-3.1)	1 (0.5-45.7)	1 (0.5-6)
	Simulated	*1.3 (0.3-1.8)*	*1.3 (0.3-1.8) [1.28]*	*1.3 (0.3-1.8) [1.28]*	*1.3 (0.3-1.8) [1.28]*	*1.3 (0.3-1.8)*	*1.3 (0.3-1.8)*
	PE (%)	*+30*	*-38 to +30 [-39 to +28]*	*+30 [+28]*	*+63 [+60]*	*+30*	*+30*

n/a, not available

[a]The simulated value in brackets are the predicted value and prediction error from GastroPlus™ of one simulated subject

[b]*PE, prediction error (%)* = [(predicted-observed)/observed] x 100

[c]Values are the median (range) for T_{max} and arithmetic mean (CV%) for all other parameters

TABLE 6

Clinically observed and Simcyp model-predicted pharmacokinetic parameters of panobinostat after three times a week (Monday, Wednesday, Friday) dosing for 2 weeks.

PK parameter	**Study**	**Dose**					
n		**15 mg**	**20 mg**	**30 mg**	**40 mg**	**60 mg**	**80 mg**
	B2101	3	18	4			
	B2102		8	12	22	17	4
	Simulated	*100*	*100*	*100*	*100*	*100*	*100*
C_{max}	B2101	13.2 (58)	28.8 (62)	17.3 (61)			
ng/ml	B2102		33.6 (49)	38.4 (61)	41.6 (88)	51.8 (56)	69.6 (39)
	Simulated	*16.7 (126)*	*22.4 (126)*	*33.9 (126)*	*45.6 (126)*	*69.6 (126)*	*94.2 (126)*
	PE (%)[a]	*+27*	*-33 to -22*	*-12 to +96*	*+10*	*+34*	*+35*
AUC_{0-48}	B2101	149 (48)	264 (56)	235 (62)			
ng × h/ml	B2102		245 (87)	280 (59)	271 (59)	306 (50)	369 (52)
	Simulated	*180 (47)*	*242 (48)*	*368 (48)*	*498 (48)*	*765 (48)*	*1044 (49)*
	PE (%)	*+21*	*-8 to -1*	*+31 to +57*	*+84*	*+150*	*+183*
T_{max}[b]	B2101	1	1	2.1			
h	B2102		1 (0.5-2.1)	2 (0.7-4.0)	1.1 (0.5-4.0)	1.1 (0.5-6.0)	1.5 (0.7-2.0)
	Simulated	*1.3 (0.3-1.7)*	*1.3 (0.3-1.8)*	*1.3 (0.3-1.8)*	*1.3 (0.3-1.7)*	*1.3 (0.3-1.8)*	*1.3 (0.3-1.8)*
	PE (%)	*+30*	*+30*	*-38 to -35*	*+18*	*+18*	*-13*

[a] *PE, prediction error (%)* = [(predicted-observed)/observed] x 100

[b] Values are the median (range) for T_{max} and arithmetic mean (CV%) for all other parameters

TABLE 7

Clinically observed and Simcyp model-predicted pharmacokinetic parameters of panobinostat administered as a single oral 20 mg single dose with (1 h after 4th KTZ dose) and without KTZ 400 mg orally dosed once a day for 5 days.

PK parameter[a]		**Panobinostat alone**	**Panobinostat + KTZ**	**Geometric mean ratio (90% CI)**
C_{max} *ng/ml*	Observed[b] (*n* = 14)	18.52 (42.6)	29.98 (93.3)	1.6 (1.2-2.2)
	Predicted (*n* = 100)	9.67 (146)	16.5 (154)	1.7 (1.6-1.8)
	Prediction error (%)[c]	*-48*	*-45*	*6*
$AUC_{0-\infty}$ *ng × h/ml*	Observed (*n* = 11-12)	133.0 (39.9)	220.7 (54.6)	1.8 (1.5-2.2)
	Predicted (*n* = 100)	225 (48)	401 (48)	1.8 (1.7-1.9)
	Prediction error (%)	*+69*	*+82*	*0*

[a]Values are the geometric mean (CV%)
[b]Observed values are from Hamberg et al., 2011
[c]*Prediction error %* = [(predicted-observed)/observed] x 100

TABLE 8

Clinically observed and Simcyp model-predicted pharmacokinetic parameters of panobinostat on Cycle 1 Day 8 (in the absence of DEX) and on Cycle 2 Day 8 (in the presence of DEX).

PK parameter[a]		**Panobinostat alone**	**Panobinostat + DEX**	**Geometric mean ratio**
C_{max} *ng/ml*	Observed[b] (*n* = 12-15)	9.5 (60.4)	8.1 (90.3)	0.85
	Predicted (*n* = 100)	12.3	13.6	0.90
	Prediction error (%)[c]			
AUC_{0-24} *ng × h/ml*	Observed (*n* = 12-15)	61.8 (60.9)	47.5 (76.8)	0.77
	Predicted (*n* = 100)	117	99.3	0.85
	Prediction error (%)			

[a]Values are the geometric mean (CV%)
[b]Observed values are Mu et al., 2016 and San-Miguel et al., 2013
[c]*Prediction error %* = [(predicted-observed)/observed] x 100

DMD Fast Forward. Published on September 14, 2017 as DOI: 10.1124/dmd.117.076851
This article has not been copyedited and formatted. The final version may differ from this version.

TABLE 9

Simcyp model-predicted pharmacokinetic parameters of panobinostat administered as a single oral 20 mg dose on day 7 with and without RIF 600 mg orally dosed once a day for 14 days.

PK parameter[a]		**Panobinostat alone**	**Panobinostat + RIF**	**Geometric mean ratio (90% CI)**
C_{max}[a] *ng/ml*	Predicted (*n* = 100)	9.67 (146)	4.34 (149)	0.45 (0.41-0.49)
$AUC_{0-\infty}$ *ng × h/ml*	Predicted (*n* = 100)	231 (47)	80.1 (63)	0.35 (0.32-0.38)

[a]Values are the geometric mean (CV%)

TABLE 10

Simcyp model-predicted pharmacokinetic parameters of MDZ administered as a single oral 5 mg dose on day 15 with and without multiple administration of panobinostat 20 mg three times a week (Monday, Wednesday, Friday) for 2 weeks.

PK parameter[a]		**MDZ alone**	**MDZ + panobinostat**	**Geometric mean ratio (90% CI)**
C_{max} *ng/ml*	Predicted (*n* = 100)	14.5 (57)	15.1 (56)	1.04 (1.03-1.04)
$AUC_{0-\infty}$ *ng × h/ml*	Predicted (*n* = 100)	56.2 (64)	58.7 (64)	1.04 (1.04-1.05)

[a]Values are the geometric mean (CV%)

DMD Fast Forward. Published on September 14, 2017 as DOI: 10.1124/dmd.117.076851
This article has not been copyedited and formatted. The final version may differ from this version.

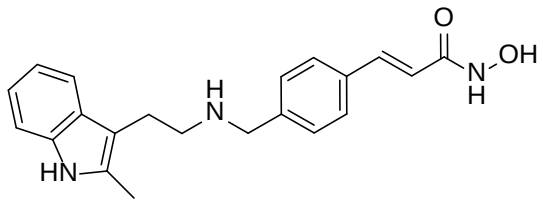

Figure 1

DMD Fast Forward. Published on September 14, 2017 as DOI: 10.1124/dmd.117.076851

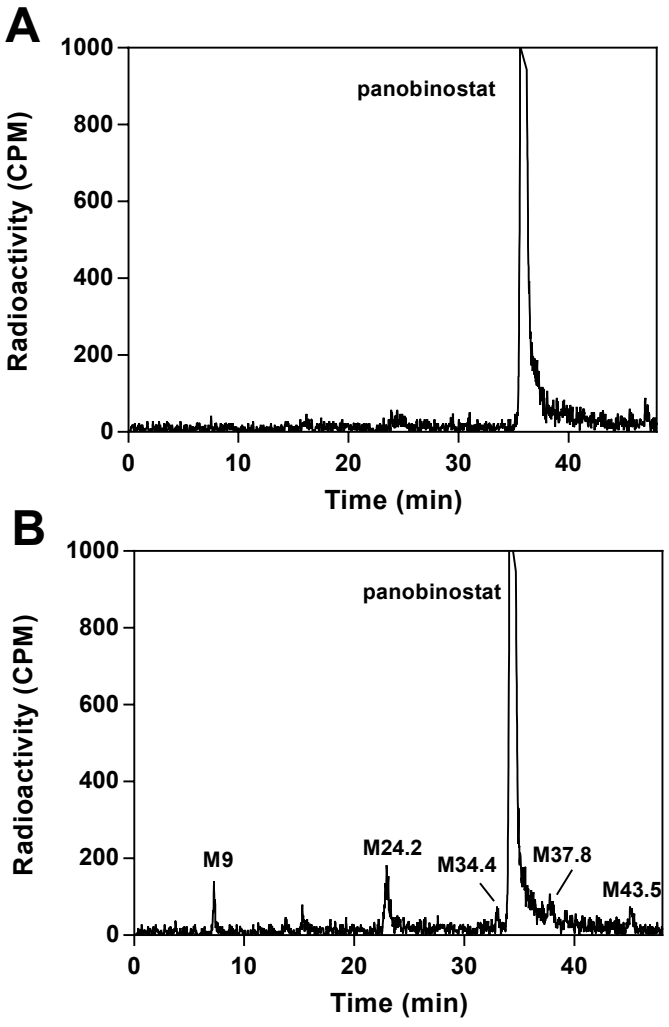

Figure 2

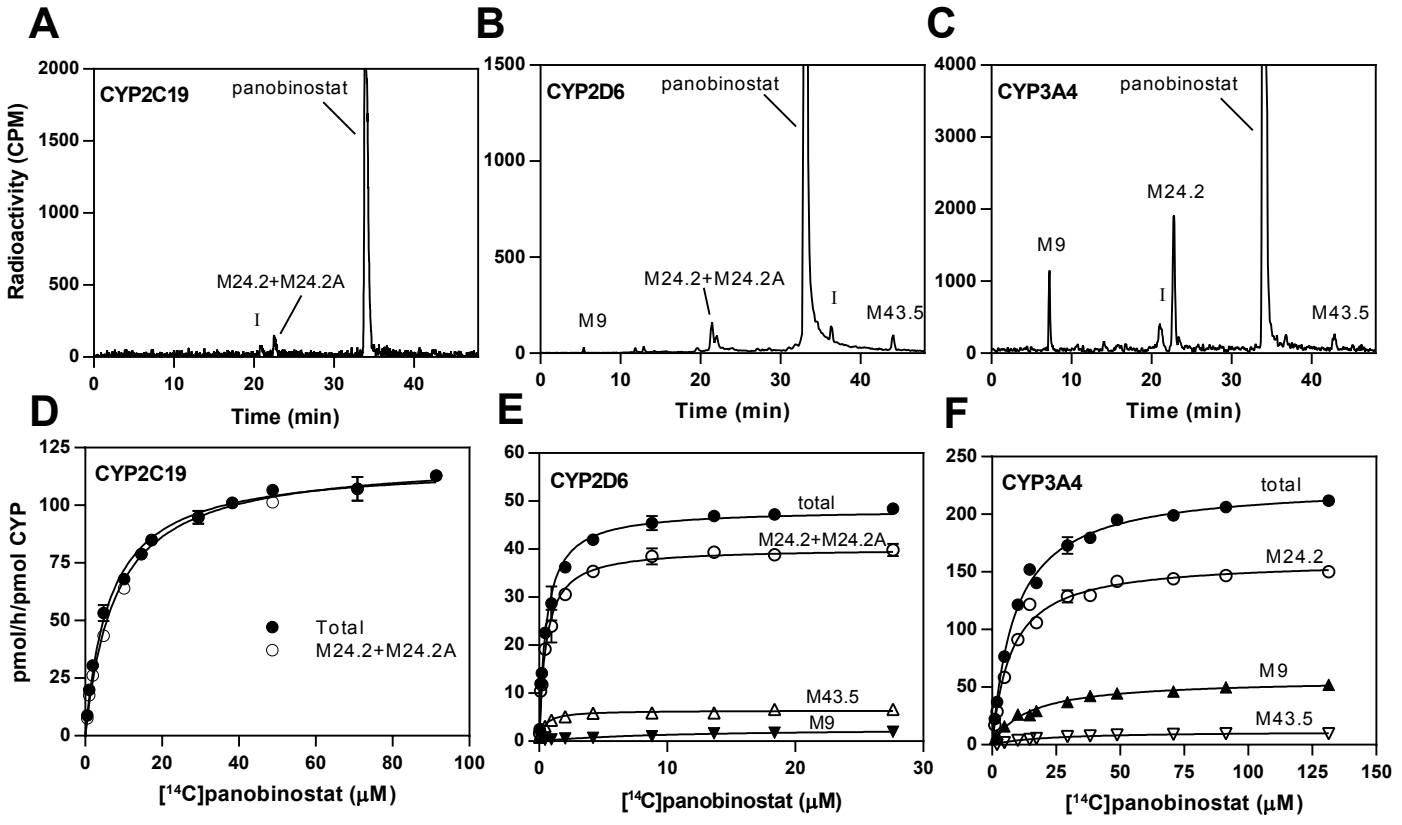

Figure 3

DMD Fast Forward. Published on September 14, 2017 as DOI: 10.1124/dmd.117.076851
This article has not been copyedited and formatted. The final version may differ from this version.

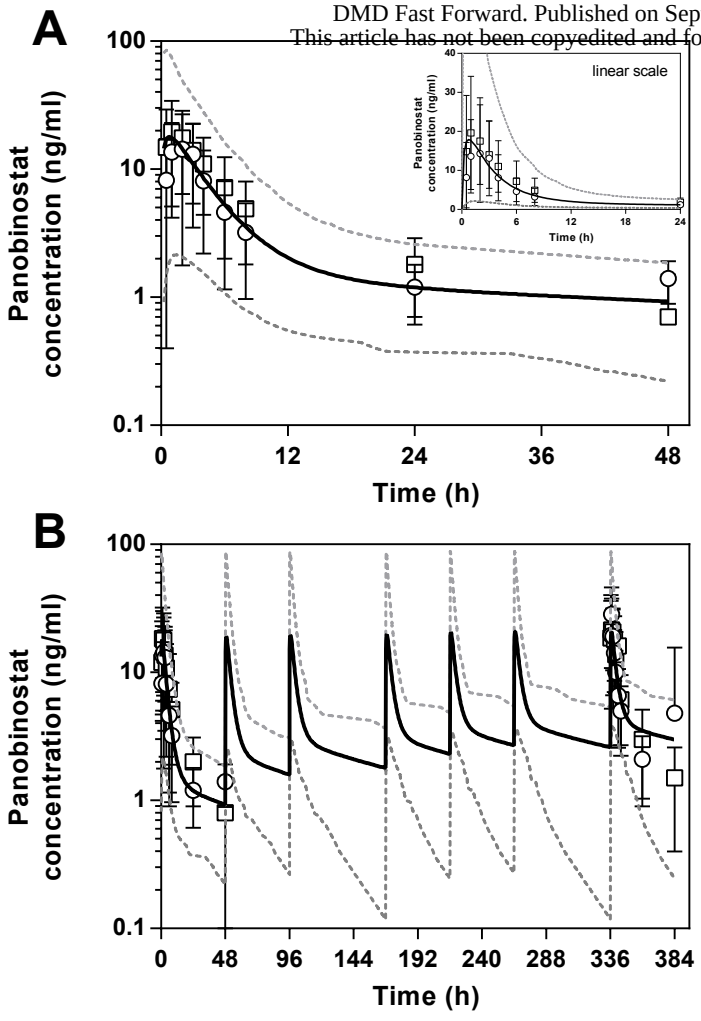

Figure 4

DMD Fast Forward. Published on September 14, 2017 as DOI: 10.1124/dmd.117.076851
This article has not been copyedited and formatted. The final version may differ from this version.

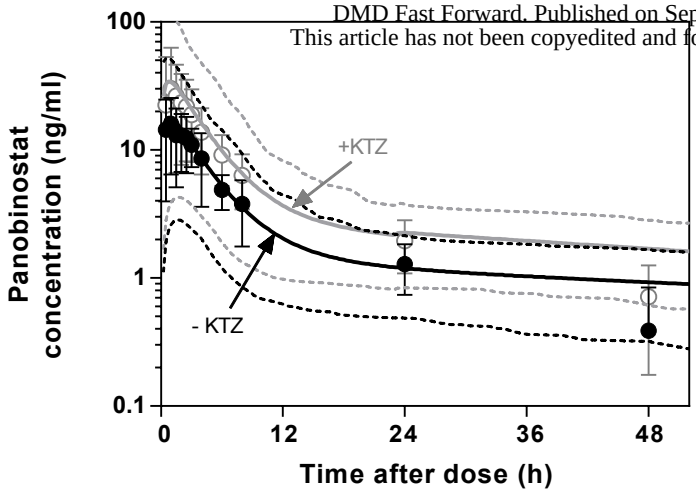

Figure 5

DMD Fast Forward. Published on September 14, 2017 as DOI: 10.1124/dmd.117.076851
This article has not been copyedited and formatted. The final version may differ from this version.

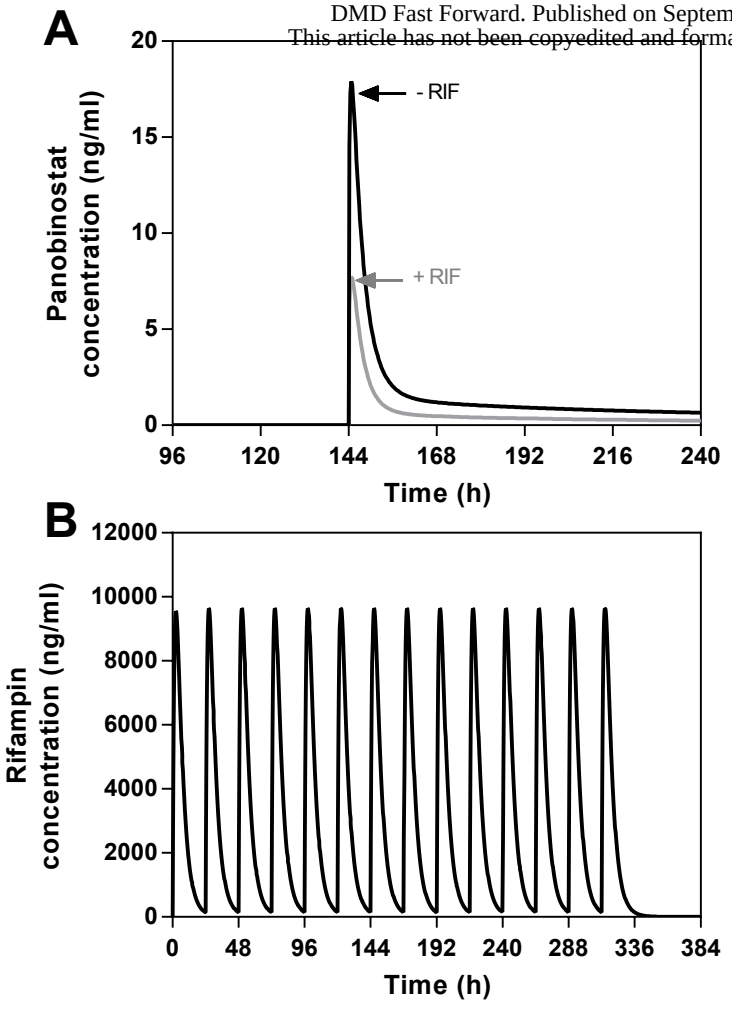

Figure 6

DMD Fast Forward. Published on September 14, 2017 as DOI: 10.1124/dmd.117.076851
This article has not been copyedited and formatted. The final version may differ from this version.

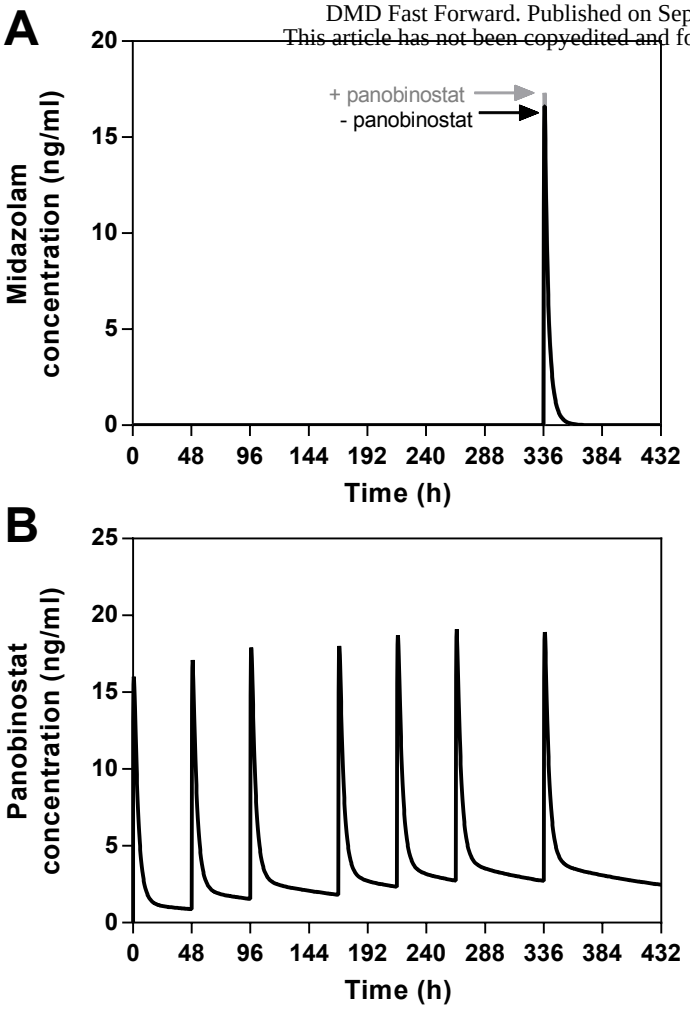

Figure 7

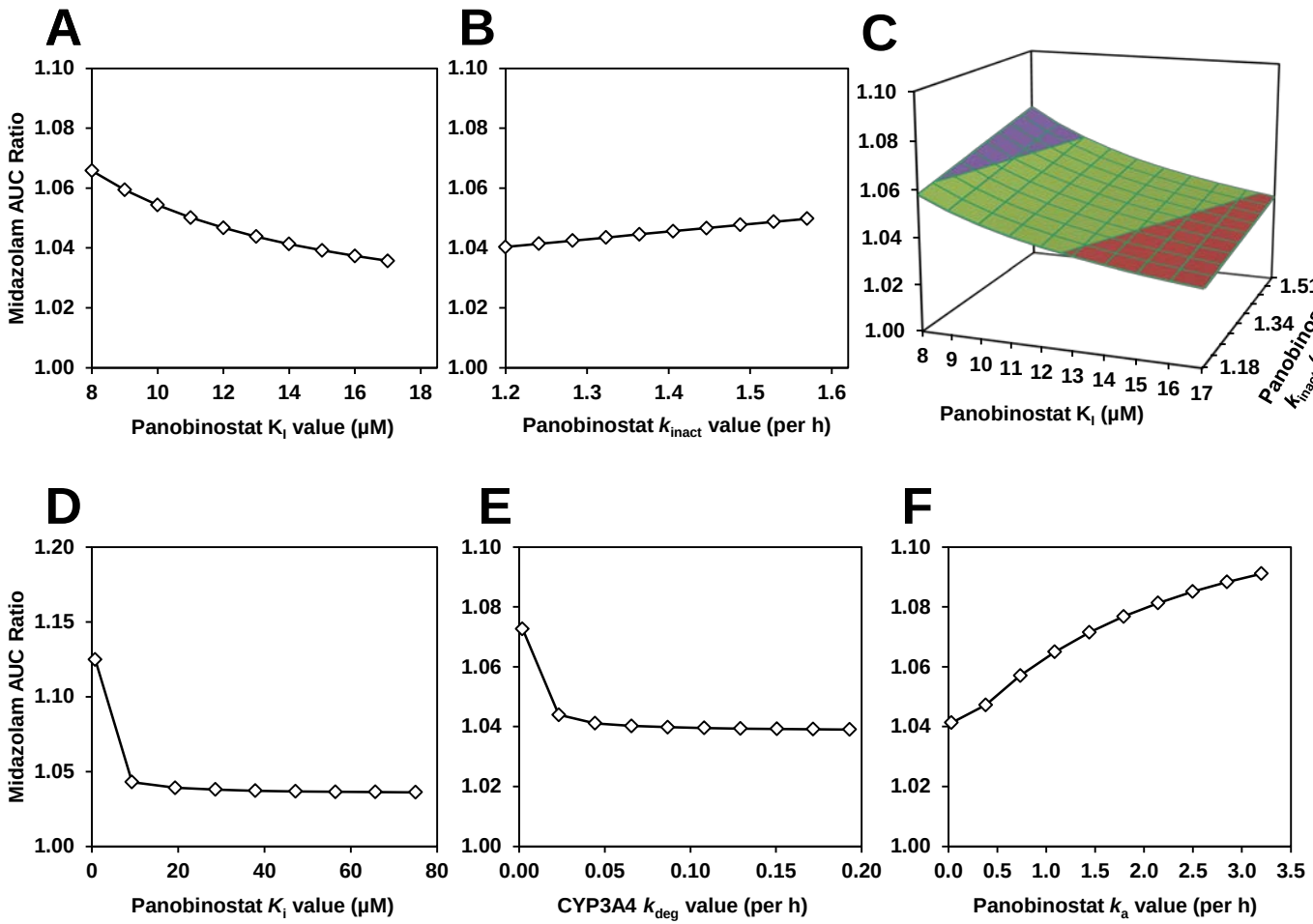

Figure 8

DMD Fast Forward. Published on September 14, 2017 as DOI: 10.1124/dmd.117.076851
This article has not been copyedited and formatted. The final version may differ from this version.

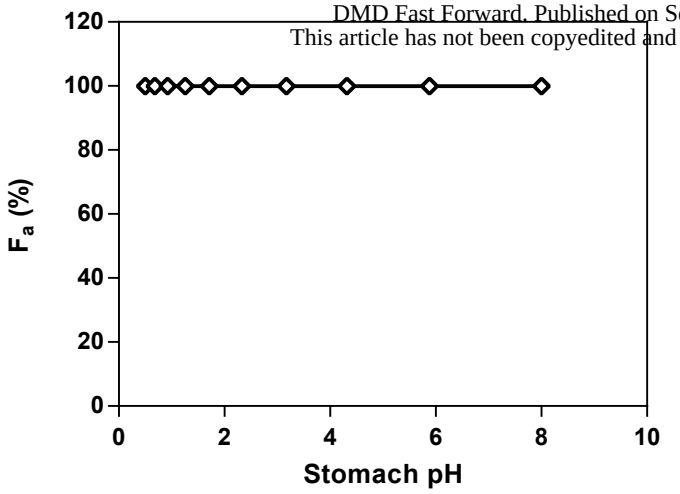

Figure 9